Sensors and Actuators A 296 (2019) 155–177

Contents lists available at ScienceDirect

Sensors and Actuators A: Physical

journal homepage: www.elsevier.com/locate/sna

Review

Recent advances in non-contact force sensors used for micro/nano manipulation

Haoyan Zang [a], Xianmin Zhang [a,*], Benliang Zhu [a], Sergej Fatikow [a,b]

[a] Guangdong Key Laboratory of Precision Equipment and Manufacturing Technology, South China University of Technology, Guangzhou 510640, China
[b] Division Microrobotics and Control Engineering, University of Oldenburg, 26129 Oldenburg, Germany

ARTICLE INFO

Article history:
Received 27 April 2019
Received in revised form 10 June 2019
Accepted 3 July 2019
Available online 8 July 2019

Keywords:
Micro/nano manipulation systems
Micro-force sensors
Optical fiber sensors

ABSTRACT

Micro/nano manipulation for both mechanical and biological structures is currently a popular research field. To protect small-scale structures and acquire their mechanical properties, a micro-scale force sensor is needed. This paper focuses on reviewing the research on non-contact micro-force sensor parts that can be integrated in this manipulation system. The content involves the structure, working principle, resolution and sensitivity of different force sensor parts, including electrical and optical force sensors. The electrical force sensors include piezoresistive, piezoelectric, capacitive, electrothermal and strain gauge-based types; while the optical force sensors focus on but are not restricted to the optical fiber-based force sensors and the vision-based sensing systems. All of these sensors are analysed and compared. Electrical force sensors are currently widely used but are restricted by the sensing properties and size; optical force sensors have high sensitivity, small structure and anti-electromagnetic-interference properties, but they are hardly applied in micro/nano manipulation systems for force measurement. As a result, optical force sensors may become the new generation of sensors that can be integrated with micro/nano manipulation systems.

Contents

* Corresponding author.
E-mail address: zhangxm@scut.edu.cn (X. Zhang).

https://doi.org/10.1016/j.sna.2019.07.007
0924-4247/

1. Introduction

Micro/nano manipulation is a popular interdisciplinary research field of this century. This approach is common for the fabrication of three-dimensional (3D) microstructures, the movement of nanostructures, the transportation and motion control of particles and, especially applications in biology [1,2]. Based on this technology, manipulation and characterization of biological cells, such as cell transfer, isolation, immobilization and injection have been widely used in many biological applications over the past decade [3].

As the handled biological cells can be easily damaged, the capability of precisely measuring small forces at the micro/nanoscale is necessary for providing force feedback during manipulation [4]. The measurement of force can also be used for the mechanical characterization of cells since genetic mutations and pathogens can result in changes to cell mechanical properties such as elasticity and viscosity [5]. In [6], changes in the mechanical properties of mouse zona pellucida post fertilization were tested for investigating the hardening process. Other than biological cells, force measurement is essential for sample protection and mechanical properties detection of micro/nano samples. Additionally, the force sensing system is vital for the experimental verification of the micro-force theoretical model.

Different kinds of micro-force sensors were designed during the past decades, including piezoresistive, piezoelectric, capacitive, and electrothermal sensors and those based on visual detection. Reference [7,8] demonstrated two kinds of triaxial piezoresistive micro-force sensors with millinewton resolution, while reference [9,10] presented two piezoresistive force sensors with the piezoresistance attached to the membranes. In [11,12], force sensors were constructed using the polyvinylidene fluoride(PVDF) sensing material by measuring the electric charge of the PVDF membrane. Beyeler et al. [13] devised a six-axial force sensor using seven capacitors with a micronewton resolution. Bulut Coskun et al. [14] designed a micro-electrothermal force that used feedback control to nullify displacements within the device with a high resolution of 7.8 nN. Rajagopalan et al. [15] put forward a displacement-based force sensor with the resolution of 50 pN. The force was obtained by optically measuring the displacement of the probe with respect to a fixed reference beam.

All of these abovementioned sensors are considered as contact force sensors because one part of the sensors is in direct contact with the surface of samples. There is no specific definition about the “contact sensors” and “non-contact sensors”, as the definition method is so straightforward. But they do differ from each other, as those contact force sensors cannot realize simultaneous manipulation and measurement process. Moreover, there is insufficient space to place an extra force sensor besides the end-effectors into the manipulation system because micro/nano manipulation systems are always under an optical microscope or inside an electron microscope cavity. Therefore, it is better to integrate the force sensors with micro-manipulators as a part to realize the synchronization of manipulating and measuring and save space for the system. Under this condition, the sensors do not contact the samples but as a part of the manipulating system with only the end-effectors touching the samples. Thus, they can be considered as non-contact types.

The sensing methods have developed with advances in physical science. The commonly used sensors currently are those utilizing electrical theory, comprising piezoresistive, piezoelectric, electrothermal and capacitive sensors [16]. They convert mechanical signals into electrical signals involving voltage, electric current, resistance and capacitance. Moreover, force sensors based on optics are newly used approaches but are hardly developed. Most micro-force sensors based on optical theory utilize the vision metrology by detecting the deformation of related elements. Other sensors measure the force on the basis of optical theory such as optical beam deflection, yet they are barely applied to micro/nanoscale force measurement.

These referenced sensing theories can be integrated with different manipulators of micro/nano manipulation systems involving grippers and tweezers. Chen et al. designed a microgripper using a triangulation amplification-based mechanism as a compliant orthogonal displacement amplification mechanism [17,18] and then optimized the framework of the microgripper to maximize the grasping movements [19]. Sun et al presented a two-grade amplification mechanism adopting the integration of flexure hinge and flexure beam [20]. Andersen et al. [21] and Chen et al. [22] put forward a kind of monolithic microgripper for small object gripping. In addition, instruments such as optical tweezers, magnetic tweezers and cantilevers of an atomic force microscope (AFM) are also available for mechanical characterization of micro/nanoscale samples, while they are not particularly suitable compared to MEMS-based devices [23]. The ends of cantilevers can even bond with carbon nanotubes or other nanowires as force sensors [24,25]. Among all these instruments, AFM cantilevers achieve the most usage next to grippers and tweezers. In addition, the traditional sensing method for the AFM is to detect the static deformation of the cantilever as it approaches the sample surface, while the deformation is sensed with a position-sensitive detector by detecting the deflection of a weak laser beam that is reflected off its backside [26]. As the AFM cantilevers have been applied on more occasions, different sensing methods have also been put forward.

The following content is a detailed introduction to different kinds of non-contact force sensors that can be integrated with micro/nano manipulation systems. The organization is as follows. Section 2 presents the theories and applications of electrical micro-force sensors, involving piezoresistive, piezoelectric, electrothermal and capacitive sensors. Many manipulators that are integrated with these mechanical micro-force sensors are outlined in this section. Section 3 is an introduction to micro-force sensing methods based on optical theory involving optical waveguide theory, visual measuring techniques and other relevant methods. Section 4 discusses the summary of these micro-force sensors and comparisons of the parameters such as sensitivity and resolution, and then talk about the common fabrication methods as well. Finally, Section 5 presents the conclusion of non-contact force sensors for micro/nano manipulation systems.

2. Electrical micro-force sensors

Mechanical micro-force sensors are the most popular non-contact force sensors integrated with microgrippers, micro-tweezers and even AFM cantilevers, showing the importance of micro/nano manipulation systems. This section introduces these

different kinds of sensors, including piezoresistive, piezoelectric, electrothermal and capacitive sensors. Additionally, strain gauges are discussed as a kind of widely used sensing element.

2.1. Piezoresistive sensors

Piezoresistive sensors are based on the bulk resistivity varying with applied stress. The resistance of a resistor built into the beam will change when the cantilever is stressed with deflection [27]. This property is expressed by the following formula:

$$K = \frac{\Delta R/R}{\epsilon}. \tag{1}$$

where ΔR is the variation of the piezoresistor while R is the initial value of the piezoresistor, ϵ is the strain and K is gauge factor defined by the equation. The change in resistance is due to both the geometric effects $(1+2\nu)$ and the fractional change in resistivity $(\Delta\rho/\rho)$ of the material with strain as follows:

$$\frac{\Delta R}{R} = (1+2\nu)\epsilon + \frac{\Delta\rho}{\rho}. \tag{2}$$

where ν is the Poisson ratio and ρ is the resistivity of the piezoresistor [28].

Recent research about piezoresistive non-contact micro-force sensors is as follows. Chen et al. designed a MEMS-based side direction force sensor integrated on a four-arm structure MEMS gripper, with a resolution better than 3 μN and a sensitivity better than 72 V/N experimentally [29,30]. Duc et al. designed a force-sensing cantilever beam consisting of a silicon cantilever with sensing piezoresistors on top. The change of resistance comes from the difference in the longitudinal stress on the opposite sides of the cantilever when the sensing cantilever bends. The minimum detectable force is 770 nN and the sensitivity is up to 1.7 V/N [31]. Duc et al. put forward a two-dimensional force sensing cantilever with the resolution estimated at 21 nN and 4 nN for lateral and vertical configurations as well as a sensitivity up to 100 V/N and 540 V/N, respectively [32,33]. Reference [34] presented two integrated sensors capable of detecting the contact force for global and local sensing. The resolution, sensitivity, and range of the global sensors are 1 μN, 2.8 V/N and 3 mN, while the resolution and measuring range of the local sensor are 20 μN and 3 mN, respectively.

The piezoresistive sensors are also appropriate for AFM cantilevers as another sensing method that does not utilize the deflection of the laser beam. Early in 1993, the piezoresistive detection method was devised by embedding a piezoresistive strain sensor in the AFM cantilever. The result of cantilever deformation came from the resistance change [27]. In recent years, Sierakowski et al. [35] and Majstrzyk et al. [36] demonstrated the force sensing method using piezoresistors as well as the technology of fabrication (Figs. 1).

The piezoresistive sensing theory for micro-force detection is a mature technology with a wide measuring range, high resolution, and high reliability. The sensor is maintenance-free and simple to be constructed, but there are many disadvantages as well. The structure is rigid and fragile with a high power consumption. The testing results cannot be detected easily, and because the testing is sensitive to the variation in temperature, the reproducibility is poor.

2.2. Piezoelectric sensors

Piezoelectric force sensors utilize the direct piezoelectric effect to measure strain. The direct piezoelectric effect refers to the electric charge generation of a piezoelectric material when stress is applied [37]. The basic relationship between the output voltage $V(t)$ and the micro contact force rate $\dot{F}(t)$ for the sensor is given as:

$$V(t) + \lambda\dot{V}(t) = B\dot{F}(t). \tag{3}$$

where λ and B are constants that depend on the electrical parameters and mechanical dimensions of the piezoelectric sensor. The electrical related constant λ is connected to the piezoelectric coefficient, which is the amount of charge caused by the applied force and is dependent only on the material used [38].

The piezoelectric materials that are primarily used include piezoelectric ceramic(PZT), polyvinylidene fluoride(PVDF), ZnO and macro fibre composite(MFC). Some materials are used as actuators based on the reversed piezoelectric effect, such as PZT, while others are used as sensors based on the direct piezoelectric effect. Shen et al. designed a 1D PVDF micro-force sensor integrated with a micro-gripper with sub-micronewton resolution [39]. Kim et al. put forward a PVDF-based pipette for modification characterization of the zebrafish embryo chorion with a 14.5 μN resolution [40]. Chen et al. devised a needle with PVDF films measuring the force [41]; while Huang et al. demonstrated a PVDF-based pipette used for cell injection, with a sub-micronewton resolution and sensitivity of 0.1901 mV/μN [42]. Wang and Wei et al. [43,44] devised a microinjection system with piezoelectric force sensing. The material of the sensors is composed of PVDF films as well as a hybrid of PVDF and MCF films, with the sensor resolution and sensitivity at 0.8 mN and 1.23 mV/mN, respectively. Korayem et al. [45–47] utilized a piezoelectric layer as a sensor for the AFM cantilever to reduce the size of the microscope and enhance the quality of surface topography in micro- and nanometre scales as well (Figs. 2).

The piezoelectric micro-force sensing method has a variety of advantages such as high accuracy, resolution and sensitivity as well as high dynamic range, stiffness and frequency response. The structure is small so that it can be integrated with a micro/nano system easily. However, the spatial resolution is poor because drift occurs with the presence of static forces due to the working principle of piezoelectric sensors. This kind of sensor is often applied in dynamic force sensing rather than static force sensing [48].

2.3. Capacitive sensors

Capacitive force sensors measure the force by changing the distance between the plates of comb in the capacitor. The distance change comes from the deformation of related micro handling tools caused by the force to be detected. The basic relationship between capacity and distance is expressed as

$$C = \frac{\epsilon_0\epsilon_r S}{4\pi k d}. \tag{4}$$

where S is the interaction area; ϵ_0, ϵ_r and k are the vacuum permittivity, relative dielectric constant and Cullen constant, respectively. The distance change can be calculated by the initial and varying values of the capacity.

Beyeler et al. designed a gripper integrated with a 1-dimensional micro-force sensor for manipulating micro-objects [49]. Kim et al. devised a micromanipulation system with a 2-axial force sensor on the micro-gripper. The 2-axial force sensing is performed by two sensors, where one is for contact detection with a 38.5 nN resolution, while the other is for gripping force measurement with a 19.9 nN resolution. This is the first demonstration of biological cells at the nanonewton force level and was applied in the microscale testing of swollen hydrogel microcapsules in the wet state during manipulation [50–54]. Muntwyler et al. then put forward a micro-gripper used for mechanical characterization of microscope samples with 2-dimensional force feedback. The measurement range is ±60 μN, and the resolution is 60 nN [55]. Jia et al. presented a dual sensing mode micro-gripper with a symmetrical structure

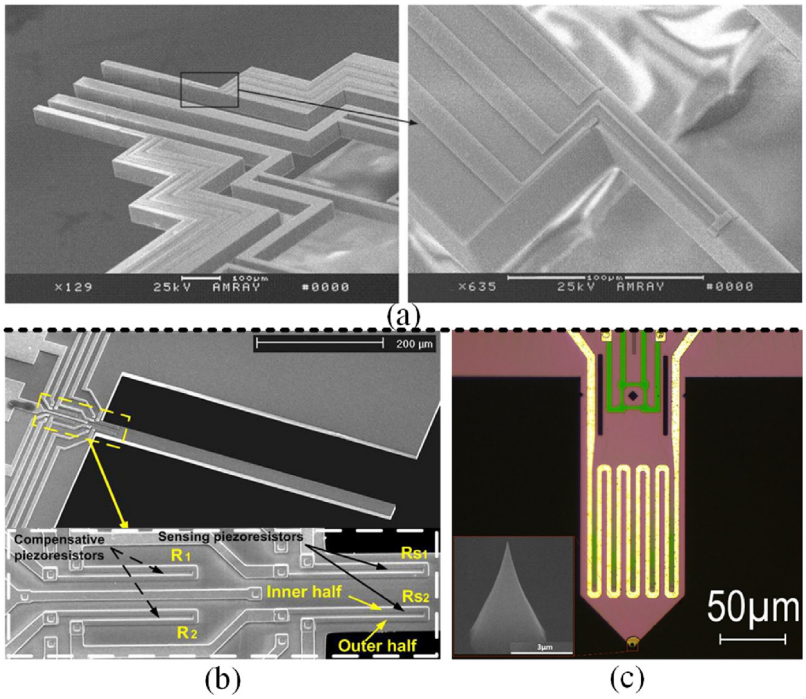

Fig. 1. (a) SEM images of the griper and the piezoresistive sensor part [29], (b) SEM pictures of 2-dimensional piezoresistive force sensor cantilever [32], (c) image of a piezoresistive active cantilever used [35].

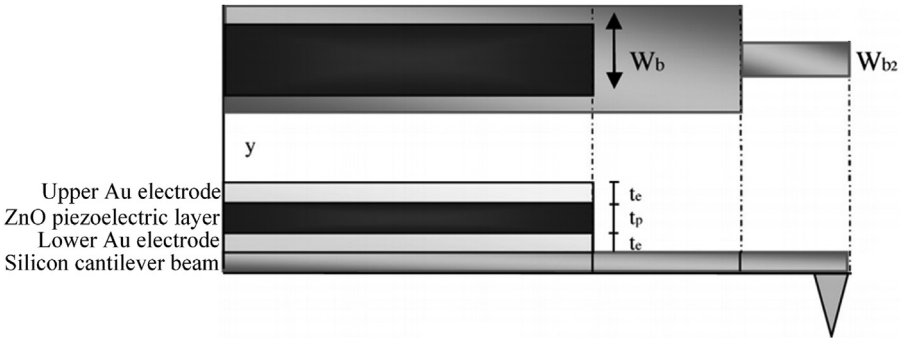

Fig. 2. Schematic of AFM cantilever with non-uniform piezoelectric layer severed as the sensor [45].

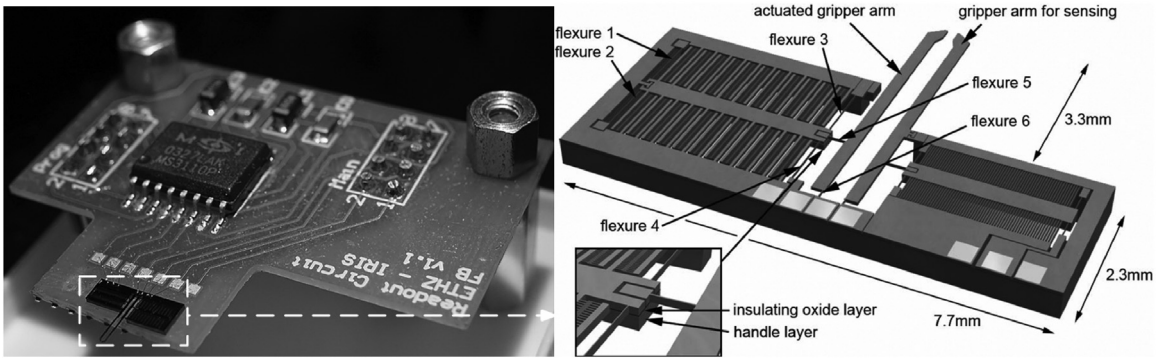

Fig. 3. Picture and solid model of the microgripper with integrated force sensor [49].

[56,57]. Juntian Qu et al. devised a micro-gripper integrated with two force sensors for microscale compression and shear testing of soft materials [58,59]. Sijie Yang et al. proposed a microgripper with two capacitive force sensors to detect a 2D micro-force [60–62] (Figs. 3 and 4).

The capacitive sensors have higher sensitivity, higher spatial resolution and lower energy consumption than other mechanical sensors. They are not sensitive to the change of the environment and have drift-free measurement capability as well. Meanwhile, the drawbacks of these sensors are sensitivity to noise and limited

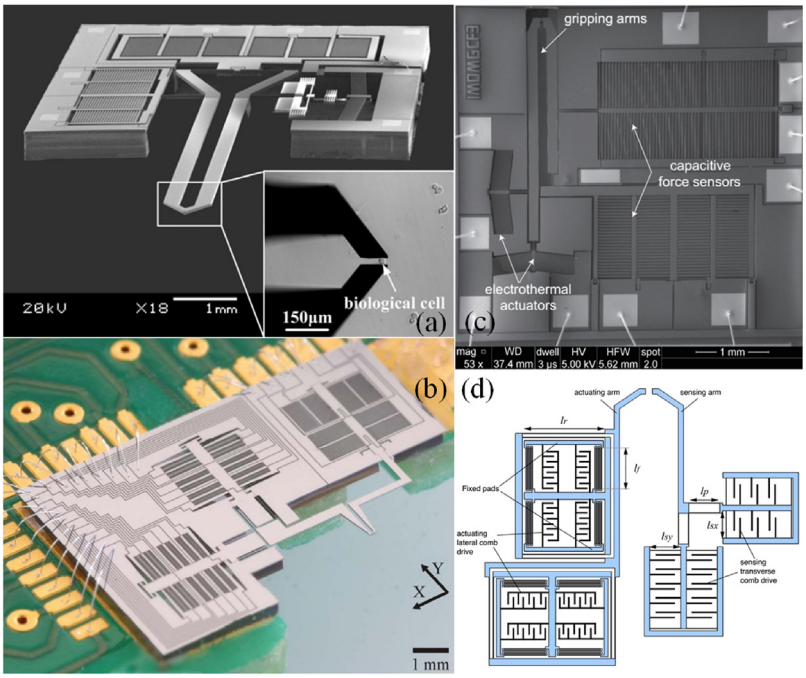

Fig. 4. (a) MEMS-based microgripper with integrated 2-axis force sensor [50], (b) Microtensile tester integrated with 2-axis capacitive micro-force sensor monolithically [55], (c) SEM photograph of a MEMS micro-gripper with 2-axis force sensor [58], (d) Schematic sketch of the micro-gripper [60].

frequency response. The sensing element structures may exhibit fatigue failure, which would cause sensitivity drifts with time [63].

2.4. Electrothermal sensors

The electrothermal sensors utilize the change of resistance caused by the temperature variation, which comes from the structure deformation. The resistance change is often detected by a Wheatstone bridge, which is popular for resistance change measurement. The relationship between the temperature variation of the resistors and force to be detected depends on the sensing structure. With different structures, the sensitivity tends to be different.

The electrothermal micro-force sensors are used less than those mentioned above. Busara Piriyanont et al. proposed a MEMS microgripper with an integrated electrothermal force sensor with a sensitivity of 1.25 μN/μm. With the force attached to the tip of micro-gripper, the sensing arm displacement induced a temperature difference between two identical resistive sensors. The temperature difference resulted in a current variation in the two resistive elements. By using a half Wheatstone bridge and an instrumentation amplifier, the current variations resulting from resistance changes are then converted to an output voltage [64]. One year later, they put forward another kind of rotary microgripper with an integrated electrothermal force sensor with a sensitivity of 0.558 V/μN [65]. As the structure changed to a certain extent, the displacement came from the deviation of the heat sink position that was pushed by the sensing arm. This deviation induced a difference in the heat fluxes from the two beams, creating differential changes in their temperature. The temperature changes resulted in differential resistance variations, which were converted into output voltages [66]. Sijie Yang et al. also devised an electrothermal force sensor integrated micro-gripper with a similar principle, exhibiting a compact structure [67] (Fig. 5).

The electrothermal sensing method has a high resolution, a simple structure and a small dimension, while these are the advantages of all mechanical sensing methods mentioned above. However, the working temperature is relatively high compared with the others. In addition, the low response speed and large consumption also restrict the utilization of this kind of force sensor.

2.5. Strain gauge sensors

Strain gauge-based force sensing is one of the most common methods to measure a micro-force and has been commercialized. Strain gauge employ various working principles, but the most used method is on the basis that the external force changes the geometrical dimension of the sensing conductor, resulting in the resistance value variation. This kind of strain gauge contains an insulated flexible backing that supports a metallic foil pattern. The working performance is evaluated by the gauge factor, which is also named the strain coefficient of resistance:

$$GF = \frac{\Delta R/R}{\epsilon}. \tag{5}$$

The optical fibre-based strain gauge is another kind of strain gauge based on the principle that measures the phase shift between two sinusoidal modulated light signals that propagate through two optical fibres or the fibre Bragg gratings. In particular, the related content will be referred to in the next section about optical sensing methods. In this section, the introduction of sensing methods focuses on the mechanical sensing method. The following discussion will describe the application of these two kinds of methods in stain gauges.

Weihai Chen et al. put forward a micro-gripper with strain a gauge on it to measure the force of grasping [68]. Wang et al. designed a gripper using two strain gauges fixed on the two sides of the gripper as the force sensor to detect a micro-force. The accuracy of the force sensor system is 91 mN, and the resolution is 143 mN [69]. Qingsong Xu et al. presented a micro-gripper with strain gauges on the side of the tip, and the sensitivity was 658.345 mN/mV [70]. Yi-ling Yang et al. used a pair of strain gauges fixed on the two sides of the gripper for grasp force detection with a resolution of 0.035 mN [71]. Qingsong Xu put forward a kind of dual-sensitivity and dual-range micro-gripper using a semiconductor strain gauge for force measurement. The resolution of the

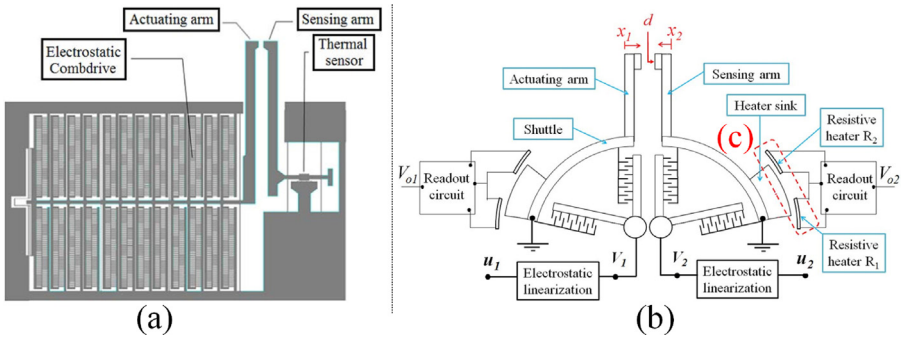

Fig. 5. (a) Model of the MEMS micro-gripper with electrothermal force sensor [64], (b) The schematic of MEMS rotary micro-gripper with (c) integrated electrothermal sensor [66].

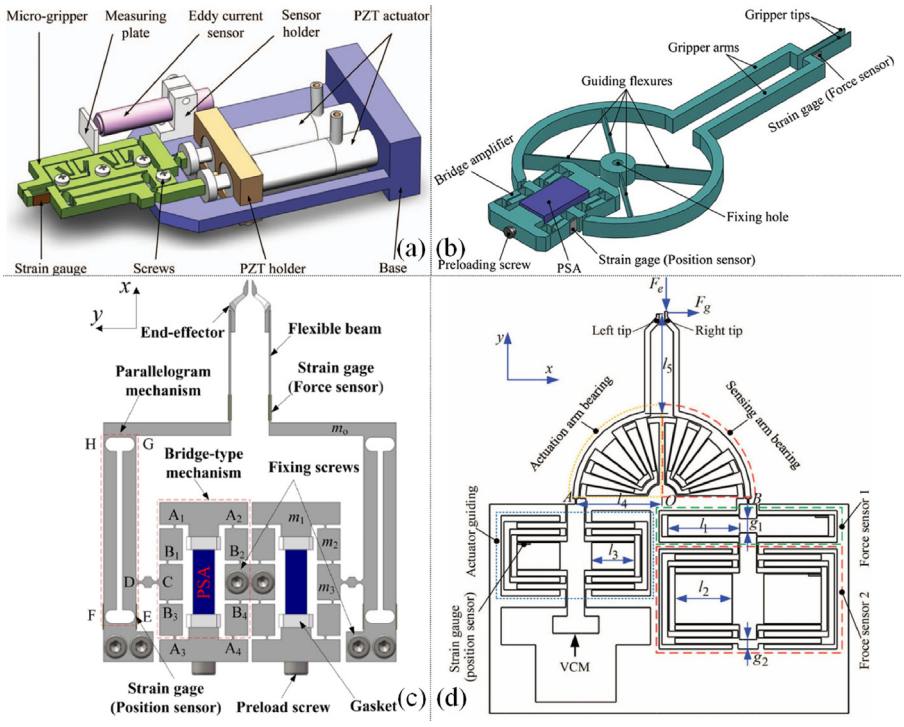

Fig. 6. Model of strain gauge based force sensor integrated on (a–d) micro-grippers [68,70–72].

two force sensors is 0.31 mN and 20.51 mN, and their sensitivity is 3.34×10^{-5} V/mN and 1.65×10^{-7} V/mN, respectively [72]. Guangwei Wang et al. presented a micropipette used for a microinjection system with strain gauges for force detection, of which the sensitivity reached 14.204 mN/mV, the resolution was 50 μN and the range was 98.1 mN [73] (Fig. 6).

This kind of micro-force sensing method appears to have a high signal-to-noise ratio and wide measuring range. Furthermore, the structure is compact and low cost. However, it is susceptible to humidity and ambient temperature. The nonlinearity of the result has also restricted the application of strain gauges in force sensing.

3. Optical micro-force sensors

Optical sensors based on MEMS technology have received increased attention as they present an alternative to conventional electrical sensing. The main advantages of optical sensors are typically high sensitivity, immunity to electromagnetic interference, inherent electrical safety, low hysteresis, small size and low consumption combined with good signal transmission [74–76]. Moreover, the optical sensing methods seem to be the most preferred methods considering space constraints in micromanipulation systems with high precision [77]. In this section, optical micro-force sensing methods are discussed, including optical fibre sensing methods, visual sensing technology as well as other related methods.

3.1. Micro-force sensors based on optical fibres

Optical fibres are the most common three-dimensional optical waveguides, which are defined as a dielectric structure that transports energy at wavelengths in the infrared or visible portions of the electromagnetic spectrum [78]. While being transported in the optical waveguides, the ray is easily affected by surrounding environments. Changes in the surrounding environment finally result in the variation of light intensity, phase, wavelength or polarization state. To detect the micro-force of the micromanipulation system without contact, the fibre sensing system can be attached to the deformed region of the manipulator by transforming the deformation to an applied force. This deformation is transferred by the sensing system into its variation of light intensity, wavelength or

phase, utilizing the theory of the bending loss, the photo-elastic effect or the principle of interferometry, respectively.

However, the optical fibre micro-force sensing methods were not well developed for several reasons. First, a relatively short amount of time has been spent on this research even though fibre sensing is not a new research field, and most of which focus has been on the macro applications such as monitoring of underground mines [79,80], experimentally pre-stressed concrete [81], rock cracking [82], overhead transmission conductors [83] and even debris flow [84]. Second, the fibre sensors are suitable for multi-parameters measurement, including refractive index [85], gas [86], humidity [87], liquid hydrostatic pressure [88], temperature [89], magnetic field [90]and current [91], some of which are not easily detected by other kinds of sensors; therefore, many studies are focused on them rather than on the micro-force. Furthermore, the optical fibre sensing theory is rather difficult, and most choose other kinds of force sensing methods with relatively easier principles, such as the sensors discussed in Section 2. Last but not least, the readout of the optical setup of fibre sensors is complicated, limiting their convenient use in micro/nano manipulation systems.

To solve the problem of the complicated output setup, simplified small-size optical equipment can be used at the expense of wavelength resolution. On the other hand, the integrated-optical device introduces new approaches for the miniaturization of optical sensing systems. A sensor is called integrated optical if at least the sensing region consists of an integrated optical waveguiding system in which a sensing medium is placed close to the waveguide core as cladding [92]. Sensors based on integrated-optical structure emerged a few decades ago, such as the integrated optical temperature sensor presented in 1982 [93],but have not received much attention chiefly because of the lack of applications [94]. Integrated optics allow for minimum system size as well as cost efficiency, precise wafer-level fabrication and integration [95], and the research on integrated optical sensing is still ongoing [96]. This may be a feasible method to address the problem of the complicated outside setup of sensors used for micro/nano manipulation systems. As a result, all these optical fibre sensing methods with the potential ability for micro-force sensing are introduced next.

The following content includes the micro-force sensing theory of gratings, interferometers, the variation of fibre intensity, and the utilization of special kinds of fibres such as micro-nanometre fibre (MNF) and microstructured optical fibre (MOF) with different characteristics. The gratings are related to the photo-elastic effect as well as the principle of interferometry; the interferometers are on the basis of Mach-Zehnder interferometry and the Fabry-Perot interferometry principle; and the fibre bending loss theory utilizes the bending loss principle to detect the deformation. Micro-nano fibre and microstructured optical fibre are different from regular fibres in size and structure, and both of them can construct a similar sensing system with regular fibres.

3.1.1. Fibre Bragg grating sensors

Among the optical fibre sensors, fibre Bragg gratings (FBGs) backscattering spectrum shifts are by far the most used for measuring mechanical strain [97]. Gratings are defined as optical elements that can divide the wavefront with a uniform width and interval. By writing gratings into the core of fibres to form the spatial phase gratings, the fibre gratings can be obtained. According to the wave vector direction, the spatial period distribution and the period length, fibre gratings are classified into four basic types: fibre Bragg grating, blazed fibre grating, chirped fibre grating and long period fibre Bragg grating. Among them, the fibre Bragg grating is the most widely used one for sensors, which can reflect specific wavelength of light. By changing the parameters such as the effective refractive index and grating period, the centre wavelength of reflected light varies. In addition, the bandwidth of reflected light also changes. Both the varied wavelength and bandwidth can be detected using a spectrometer with picometre resolution, so the sensitivity is relatively high (Figs. 7 and 8)

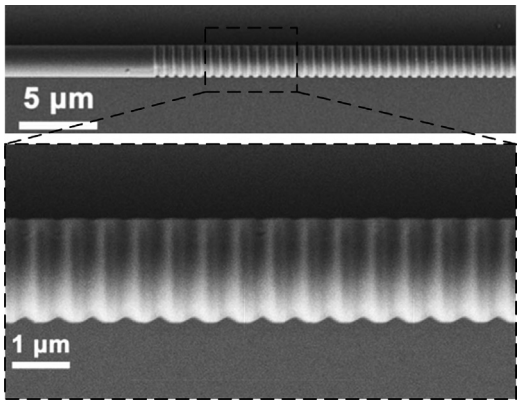

Fig. 7. SEM image of micro-fiber Bragg grating fabricated by focused ion beam [98].

According to Young's law, there is a linear relationship between the stress and strain of a spring element. Considering the fibre as a spring element, FBGs can operate as force sensors [100]. FBGs are usually designed to be the strain sensors for force sensing. Light propagating in the core of an optical fibre containing a Bragg grating will be reflected by the periodic variations of the refractive index, which comprise the Bragg grating. The reflected light will generally be out of phase and tend to cancel, except when the wavelength of the incoming radiation satisfies the Bragg condition. In this case, the light reflected by each perturbation in the grating adds constructively, and the grating couples energy from the forward propagating wave to a backward propagating reflected wave with a centre wavelength λ_B given by

$$\lambda_B = 2n_{eff}\Lambda. \tag{6}$$

When the FBGs are under tension or compression force, the grating period Λ varies as a result of length variation. In addition, the elasto-optical effect of the fibre itself makes the effective refraction index vary with the external stress state. The effect of external stress on FBG wavelength drift can be described by the following formula

$$\Delta\lambda_B = 2n_{eff}\Delta\Lambda + 2\Delta n_{eff}\Lambda. \tag{7}$$

where $\Delta\Lambda$ is the elastic deformation of fibre itself under external stress and Δn_{eff} represents the elasto-optical effect. According to the theory of the optical fibre of the light, the relative wavelength shift of FBG under uniform axial stress $-P$ is

$$\frac{\Delta\lambda_B}{\lambda_B} = (1 - p_e)\epsilon_{zz}. \tag{8}$$

where $\epsilon_{zz} = -P/E$ is the axial strain, and p_e is the effective elasto-optical coefficient, which is a constant only related to the material. When under uniform transversal stress $-P$, the relative wavelength shift is

$$\frac{\Delta\lambda_B}{\lambda_B} = [(1 - p_e) + \frac{1 - 3\nu}{4\nu} n_{eff}^2 (p_{11} + p_{12})]\epsilon_{zz}. \tag{9}$$

where ν is Poisson's ratio, $\epsilon_{zz} = 2\nu P/E$ is the axial strain, P_{11} and P_{12} are elasto-optical coefficients.

Based on the theory above, many FBG-based strain sensors were put forward. Early in 1993, a fibre-optic strain gauge system for use in structural monitoring and smart-structure applications was described, which permitted the measurement of both static and dynamic strains. The strain gauge used a fibre-optic Bragg grating sensor to measure strain with a sensitivity of 0.703 pm/$\mu\epsilon$ at a nominal centre wavelength of 821.5 nm [101]. In 2010, optical

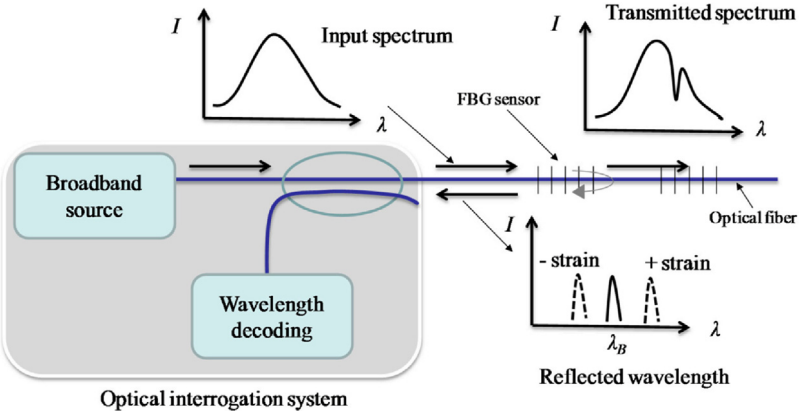

Fig. 8. Illustration of the working principle of FBG sensors [99].

fibre force sensors integrated on micro-forceps were presented for otorhinolaryngology microsurgery with the ability to measure 0.5 με [102]. In 2014, a real-time deformation monitoring system for a particle detector was described, which was made of Bragg grating sensors with the resolution of 1 με [103]. In 2015, a strain sensor based on a polyimide-coated fibre Bragg grating along with a rhombus metal structure was presented and experimentally demonstrated. The sensitivity under the compressed and stretched force is 1.821 pm/με and 1.814 pm/με respectively, and the resolution is 10 με. As the FBG was fabricated using ultraviolet (UV) light, the sensors can work under temperatures as high as 300 °C [104]. In 2018, micro-structured PMMA POF chirped Bragg gratings for strain sensing were described with a sensitivity of 0.90 pm/με. The effective bandwidth of the grating is dependent on strain and remains practically constant with respect to temperature and humidity changes [105]. In the same year, an FBG-based strain sensor with enhanced sensitivity was also presented by pasting the FBG on a substrate with a lever structure. The strain sensitivity is 6.2 pm/με, which is relatively high compared with the other FBG strain sensors above [106].

Except for these, many force sensors assembled by several FBGs were presented. In 2010, several researchers from Stanford University put forward a 3-dimensional MRI-compatible biopsy needle assembled with 3 fibre Bragg gratings [107]. In 2016, a small-diameter FBG was used as a strain sensor for real-time health monitoring with a sensitivity of 1.173 pm/με. Two FBSs with the core diameter as small as 7 μm and the cladding diameter of 80 μm were attached to a cantilever structure to construct the sensing system because small-diameter FBGs can decrease the mismatch in size between the embedded optical fibre and the composite [108]. In 2018, a 2-dimensional FBG-based micro-force sensing design for the detection of catheter tip-tissue interaction forces was put forward by mounting four optical fibres inscribed with one FBG element each on the sensor. The embedded FBG element within the suspension part was directly stretched or compressed to sense the force. The sensitivities of these two directions are 217.3 pm/N and 192.4 pm/N, respectively, and the resolution is 4.6 mN [109]. A three-dimensional force sensor based on FBG for measuring the robot plantar force was also presented for robot control. The sensitivities of three directions are 20.745 pm/N, 23.366 pm/N and 11.259 pm/N, and these sensitivities are rather lower than that of reference [110]. A fibre Bragg grating-based tri-axial force sensor with parallel flexure hinges was designed to sense the contact force and achieved the tri-axial force prediction with less than 1 g resolution. In this system, four FBGs were used with one in the centre of the parallel flexure hinges and three lateral FBGs uniformly located around the tube edge [111]. A research team from Johns Hopkins University published a series of articles describing a motorized 3-D force-sensing microneedle used for robot-assisted treatments for retinal vein cannulation. The 3D sensing system was assembled by 4 FBGs; the axial force resolution is 1.85 mN and the radial force resolution is 0.074 mN [112,113]. In 2018, four FBGs were equipped near the tip of a forceps to form a 4-DOF force/torque sensing micro end-effector. The sensor works by monitoring the grating pitch changes according to the strain change, which differs from those mentioned before [114] (Figs. 9 and 10).

In addition, as the effective refractive index is also sensitive to the temperature, many FBG-based force sensors with the ability to detect both strain and temperature were designed. In 2010, a polymer FBG-based force sensor was fabricated using UV light with the core diameter at 8.1 μm. The strain sensitivity is 1.13 pm/με, the temperature sensitivity is up to −50.1 pm/°C, and the resolution of strain and temperature is 30 με and 0.7 °C [115], respectively. In 2013, an MR-compatible biopsy needle with an enhanced tip force sense appeared. The strain resolution is 8 mN along the axial direction and 4 mN along the radial direction, while the temperature sensitivity is 23 pm/°C [116,117]. In 2017, a force sensor using a waveguide Bragg grating was developed to offset the lack of tools capable of efficiently monitoring local and dynamic contact conditions. The sensitivity of strain under 1550 nm wavelength is 8.30 pm/MPa in the radial direction and 4.16 pm/MPa in the axial direction; while the temperature sensitivity is 11.6 pm/°C [118]. In the meantime, an optical fibre Bragg grating sensor equipped on a mechanical transducer was put forward. The stain sensitivity at the wavelength of 1550 nm is 1.2 pm/με, and the temperature sensitivity is 10 pm/°C [119] (Fig. 11).

According to these examples, the FBG sensors are more sensitive to temperature than force. Therefore, methods for solving this problem are necessary. Other than some applications under uniform temperature, some studies were also focused on temperature compensation and the decoupling of temperature and force. In 2018, based on the theory of elastic mechanics and the methodology of matrices, a fibre Bragg grating-based strain sensor was designed with two fibres to realize temperature compensation. The strain sensitivity was 7.72 pm/με and −2.94 pm/με in two directions. As a result, this sensor can be used for long-term small-amplitude micro-strain monitoring in varying temperature environments for vital mechanical equipment [120]. The reference [105] is also related to temperature decoupling by detecting the effective bandwidth change that is only related to strain.

In conclusion, FBG-based micro-force sensors are common for two application fields, robots and minimally invasive surgery to date. The sensitivity of sensors used for medical treatment is higher than that for robots, as the medical objects are smaller than robotic samples. Some articles used commercial FBG strain sensors for force sensing, but more researchers designed and fabricated the FBG sen-

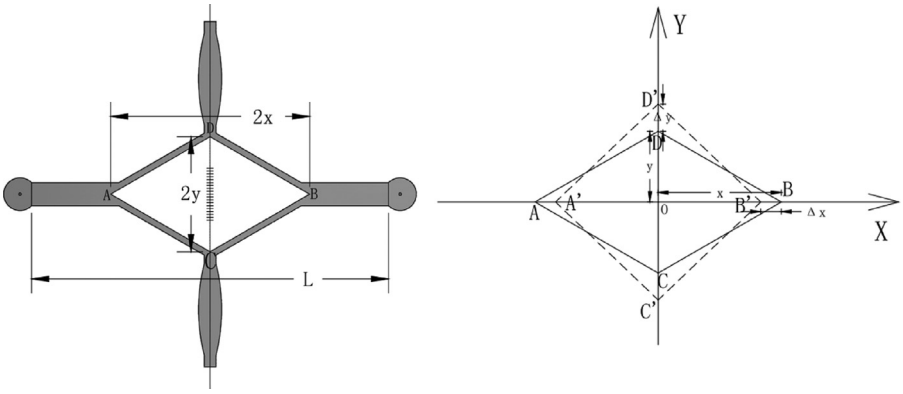

Fig. 9. Schematic diagram and principle diagram of the strain sensor [104].

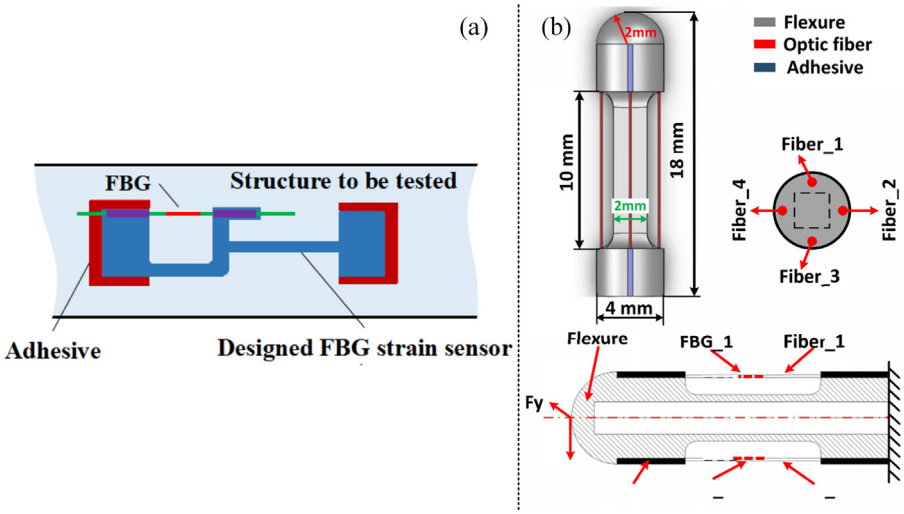

Fig. 10. (a) Top view of the sensor model [106] (b) designed structure of the proposed catheter distal force sensor and the fiber arrangement configuration [109].

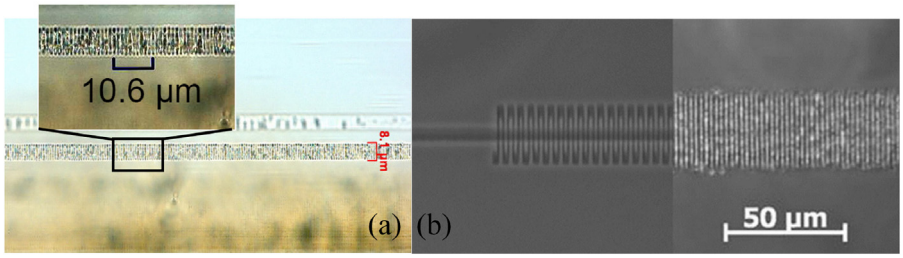

Fig. 11. Image of (a) a photo-induced index modulation of the core of POF taken by an Axioskop microscope [115], (b) a Bragg grating taken by phase contrast microscope [118].

sors for micro-force sensing. As mentioned before, some FBGs were fabricated by UV laser. In reference [121], as the FBG sensors written by UV laser exposures are not stable, FBGs fabricated by two methods were mentioned, including the femtosecond-laser and 157 nm excimer laser. These two types of lasers are powerful tools to fabricate novel in-line all-fibre fibre-optic sensors with many advantages such as direct formation, easy mass production with low cost, good reproducibility, excellent optical performance and high-temperature stability. Therefore, these systems replaced the UV light in FBG fabrication. In 2016, a small circumferential ditch of 86 μm length and 27 μm depth in the middle of a 3 mm long FBG was ablated by the femtosecond laser [122]. In 2019, a point-by-point inscription method was proposed for fibre Bragg grating fabrication using a femtosecond pulsed laser focused through a fibre polyimide coating, which achieved a high wavelength sensitivity, linearity and greater tensile strength of the FBG [123]. Except for FBGs, these fabrication methods can also be used for different kinds of Fabry-Perot interferometer strain sensors and long fibre Bragg gratings.

3.1.2. Sensors based on interferometry

Interferometry sensing methods are another commonly used approach for strain or force sensing, including Mach-Zehnder interferometry and Fabry-Perot interferometry. The Mach-Zehnder interferometer is a typical double beam interference system, while the Fabry-Perot interferometer employs a typical multiple beam interference that always forms a resonant cavity. The basic theory is shown as follows:

$$I = I_1 + I_2 + 2\sqrt{I_1 I_2}\cos\left(\frac{2\pi L \Delta n}{\lambda}\right). \quad (10)$$

$$\frac{2\pi L\Delta n}{\lambda_p} = (2m+1)\pi. \quad (11)$$

where I is the intensity of the beam, λ is the wavelength, $L\Delta n$ is the change of the light path, λ_p is the peak or trough of the wave and m is an integer that represents the order of the interference fringes.

As the light path of this interferometry is all made of optical fibres, there are two ways for the optical fibre utilization to construct the interferometer. One is fabricating the interference structure inside single fibre using structures such as air bubbles or air cavities; another is to set up the interferometers by several fibres to transmit light separately in each fibre. Some approaches even combine the interferometers with gratings together for sensing.

The reference [124] presented an optical fibre in-line Mach-Zehnder interferometer-based strain sensor by creating an inner air cavity inside a section of microfibre. The structure inside the fibre split the light propagating in the fibre into two beams, one through the inner air cavity and another along the silica wall. The two beams recombined at the cavity end, resulting in an interference fringe pattern. When the phase term satisfies a certain condition, the intensity dip appeared. By detecting the wavelength shift of the intensity dip, the strain information can be obtained. The strain sensitivity at 860 μm wavelength is 6.8 pm/με. In 2018, another reference set up an MZI-based strain sensor using two surface-relief fibre Bragg gratings [125]. The two fibres experienced different strain, which resulted in the wavelength and phase shift of two single fibres. The differential pressure was obtained by comparing two wave peaks in the spectra, and the sensitivity is 0.2 pm/MPa with temperature compensation.

The fibre Mach-Zender interferometers and fibre Bragg gratings are frequently used as optical fibre strain sensors, but they are also sensitive to temperature during strain measurements, which introduces a series of problems; however the Fabry-Perot interferometer formed by fabricating an air-cavity inside a fibre can solve the problem [126]. In this reference, a fibre FPI based on a bubble-expanded micro-cavity was investigated and exhibited a high strain sensitivity of 30.66 pm/με as well as low-temperature sensitivity of 1.2 pm/°C. In reference [127], an all-optical-fibre FPI-based sensor with the strain sensitivity of 10.3 pm/με was demonstrated, while the temperature sensitivity is 0.95 pm/°C. According to the theoretical analysis, the relationship between the cavity length change and the strain was established. Thus, the wavelength drift of the interference fringe, which is related to the cavity length, can be obtained.

In 2014, an air cavity-based FPI sensor integrated on FBG was overlapped to form the sensor for simultaneous measurement of strain and temperature. The strain sensitivity is 1.2 pm/με, and the temperature sensitivity is 11.7 pm/°C [128]. In the same year, a strain sensor based on an in-fibre FPI with an air cavity was introduced with enhanced strain sensitivity of 6.0 pm/με and low-temperature sensitivity of 1.1 pm/°C [129] (Fig. 12).

In 2015, the authors improved the property of the FPI sensors in which an air bubble was inserted by improving the air bubble creation technique. By fixing one end of the air bubble sample and attaching another end to a translation stage, the tensile strain was detected. This sensor is just one of a few that detect tensile forces. The strain sensitivity is 43.0 pm/με and the temperature sensitivity is 2.0 pm/°C [130].

In addition, there are some FPI fibre sensors without air bubbles. In 2013, the integration of an FBG and a micro external FP cavity constructed with a thin film coated on a fibre end was presented for simultaneous measurement of stress and temperature. The stress sensitivity is 8.11 pm/N and the temperature sensitivity is 200 pm/°C [131]. In 2017, a bidirectional bend sensor based on U-shaped FPI was experimentally demonstrated by splicing a section of microfibre between two cleaved standard single-mode fibre end faces serving as mirrors. The bending sensitivity is 3.544 nm/m, and the low temperature sensitivity is 1.21 pm/°C [132]. In 2018, a temperature-independent FPI and an FBG sensor were discriminated by inserting a segment of a tapered fibre tip in the capillary and subsequently splicing the other end of the capillary to a single mode fibre to form the FP cavity with the strain sensitivity of 2.1 pm/με. The sensor detects strain by changing the cavity length [133] (Fig. 13).

3.1.3. Sensors based on light energy change

The method comparing the optical energy between incident and transmission light is an easy way to perform sensing. The optical energy variation comes from the change of the light path caused by fibre bending or displacement of elements in the light path. The fibre bending loss theory is complicated, and the loss amount varies with the structure and material; in addition to the displacement of the element in the light path, the mechanical structure is determined so that the performance analysis is always accomplished according to the experimental data.

In 2016, a stretchable optical waveguide made of transparent polyurethane rubber for strain sensing in a prosthetic hand was reported, which was inserted inside each finger of the hand with a sensitivity of 0.02 dBm/cm. By detecting the loss of light intensity caused by the fibre bending, the bending amount was obtained [134]. In 2018, a bend and compression loss-based force sensor was demonstrated with enhanced sensitivity of 0.126 dB/N and 0.015 dB/N, respectively, for bend and compression. Pure skew rays were propagated through the fibre for sensitivity enhancement [135] (Fig. 14).

The sensor system comprising two sets of optical fibre pairs was put forward with the resolution to be 0.02 N. The two fibre pairs including a reference pair and a sensing pair composed the symmetrically identical bent-tip transmitting and receiving fibres that guide light from a light source to an optical detector via a reflector for each. The reflectors were affixed to a stationary support, whereas the reflector of the sensing fibre pair was attached to a flexible structure [136]. In 2017, a compliant 3-axis fibre-optic force sensor for biomechanical measurement with a similar principle was presented. However, the force measuring range was relatively large [137]. In addition, a highly sensitive FLRD strain sensor that is less sensitive to temperature by integrating an air-gap into the sensor head was demonstrated by measuring the change of ring-down time. The static strain sensitivity was 0.26 μs/με, and the low temperature sensitivity was 0.01 μs/°C [138] (Fig. 15).

3.1.4. Sensors based on micro-nano fibres

Micro-Nano fibres (MNFs) are optical fibers with diameters close to or below the vacuum wavelength of visible or near-infrared light. The reducing of the sensing structure size yields higher sensitivity, faster response, lower power consumption and better spatial resolution, and the MNFs become one of the best candidates for this purpose. With its diameter down to the sub-wavelength scale, the surrounding air is regarded as the cladding such that the index contrast between the core and cladding is relatively large. As a result, the evanescent field is very strong compared to conventional optical fibre [139].

The concept of MNF was first devised in 2003 by drawing wires from a flame-heated melt at high temperature and achieved wires with diameters down to 50 nm [140]. To date, multiple fabrication methods have been developed, including taper drawing of flame heated, laser heated or electrically heated glass fibres, drawing of flame heated bulk glass, drawing from polymer solutions and electro-spinning [141] (Fig. 16).

Because of their small size and high sensitivity, MNFs are suitable for microscale sensing. Some of MNFs are fabricated with gratings inside; others are made to be microcavities for sens-

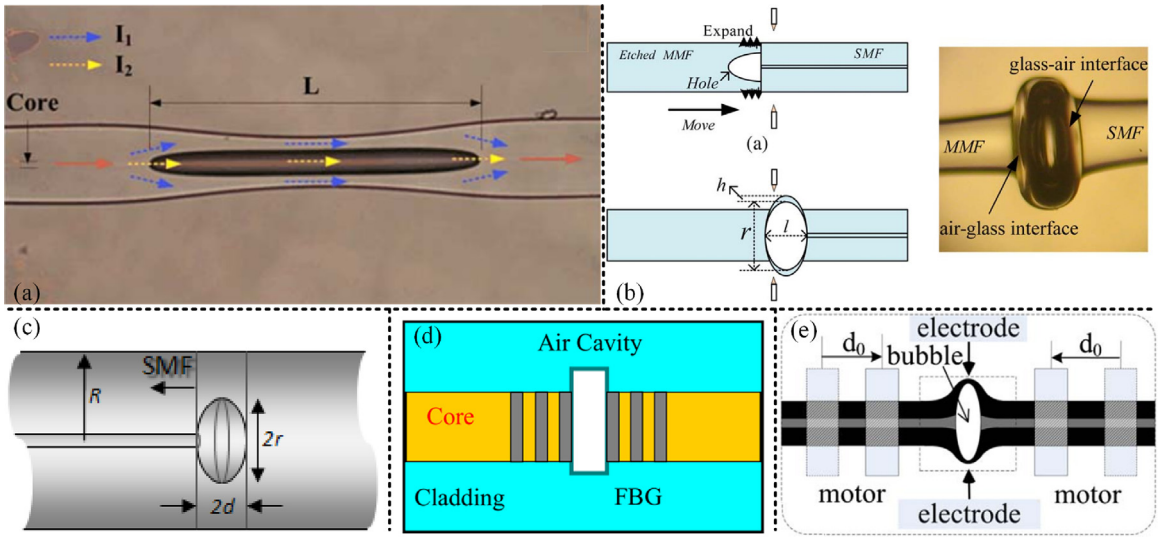

Fig. 12. (a) Hollow sphere formed after fusion splicing used for force sensing [124], (b) fabricating process and miicroscope image of the fiber FPI sensor based on the bubble-expanded air-cavity [126], (c) diagram of a Fabry-Perot interferometer force sensor with spheroidal air cavities [127] (d) structure of the MFP/SFBG [128], (e) schematic diagram of the in-fiber FPI based on an air bubble [129].

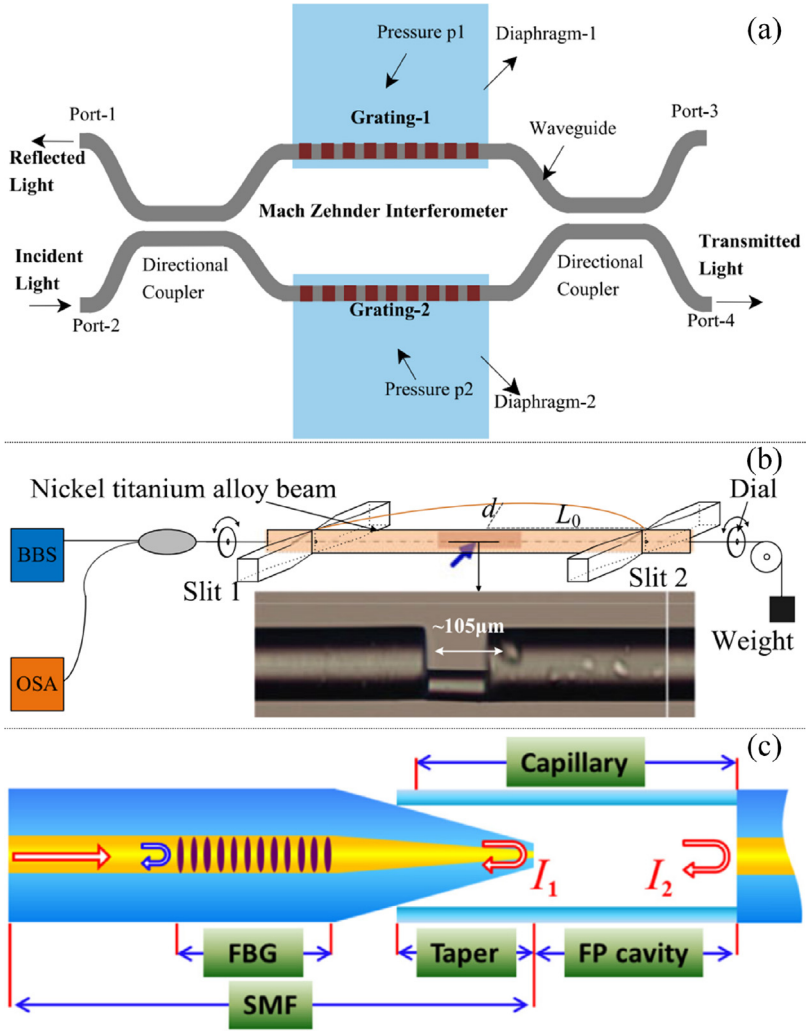

Fig. 13. (a) Schematic diagram of the differential pressure sensor [125], (b) schematic diagram of the bending sensing system [132], (c) fiber-optic strain sensor based on a hybrid structured FP interferometer and FBG [133].

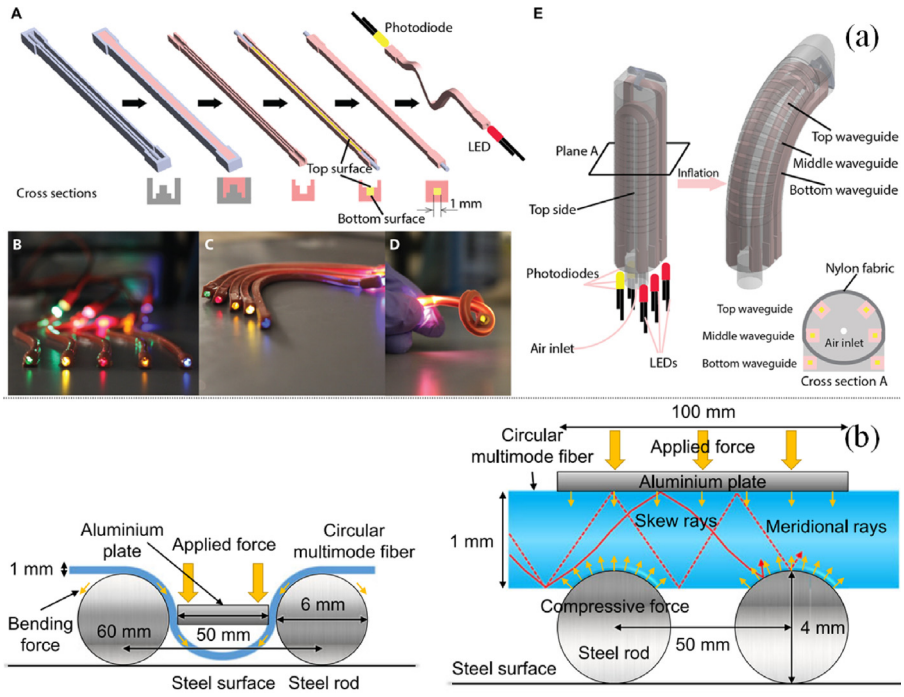

Fig. 14. (a) Stretchable waveguide fabrication and structure of the optoelectronically innervated soft finger [134], (b) schematic of the sensing fiber of bend-loss-based and compression-loss-based force sensor [135].

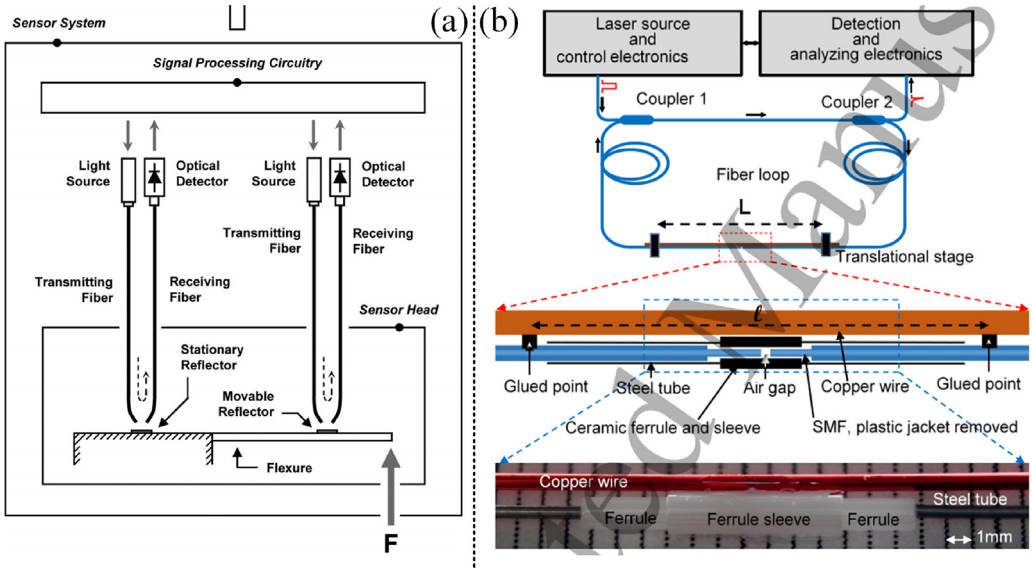

Fig. 15. (a) Schematic diagram of an optical diber force sensor system utilizing reference and sensing bent-tip fiber pair [136], (b) the FLRD ringdown strain sensor system [138].

ing. As FBGs are fabricated by forming a periodic refractive-index modulation along the fibres, a variety of microfibre Bragg grating (m-FBG) fabrication methods have been put forward. By periodic variation of the refractive index of fibre geometries, methods include chemical etching, femtosecond laser irradiation or micromachining, UV laser irradiation, focused ion beam (FIB) milling and lithography [142]. In 2011, a micro-force sensor was made by inscribing FBG in the waist of a uniformly tapered photosensitive fibre with a sensitivity of 1900 nm/N, the diameter of which was 3.5 μm. By changing the longitudinal mechanical forces applied on the fibre, the Bragg wavelength of the m-FBG changes [143]. In 2012, a microfibre tapered from standard non-photosensitive single-mode fibre inscribed with FBG by the FIB machining method was described. The force sensitivity of the microfibre Bragg grating reached 3754 nm/N with the fibre diameter down to 2.5 μm [144]. At the same time, a miniature contact force sensor based on a 30 μm diameter microfibre Bragg grating was presented. The sensitivity was 0.73 nm/N, while the excellent linearity reached a contact force of 0.65 N [146]. In 2015, a microfibre Bragg grating was fabricated under a 193 nm excimer laser with good survival ability against high temperature up to 800 °C. The diameter of the microfibre was as small as 8.5 μm and the strain sensitivity was 6.38 pm/με, while the temperature sensitivity was 14 pm/°C [147] (Fig. 17).

Due to the high evanescent field, MNFs are highly sensitive to the change of parameters of the external medium. As a result, MNF

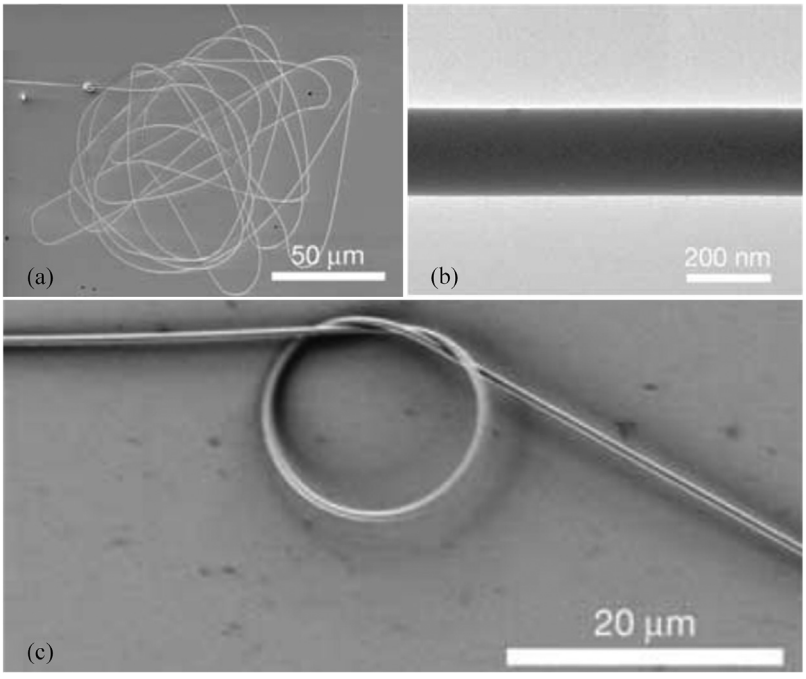

Fig. 16. (a) SEM image of a coiled 260-nm-diameter fiber, (b) TEM image of a 240-nm-diameter fiber, (c) SEM image of a 15-μm-diameter micro-ring made with a 520-nm-diameter fiber [140].

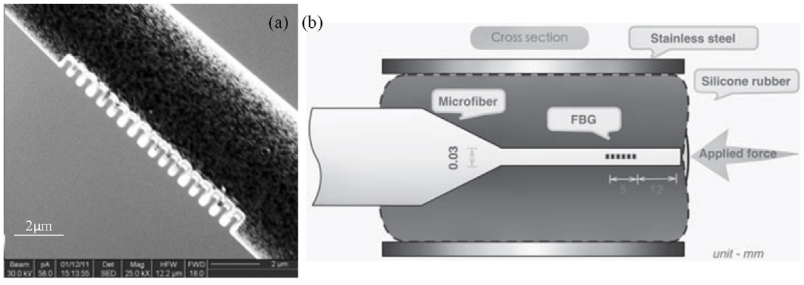

Fig. 17. (a) SEM image of micro-fiber tip grating [145], (b) schematic diagram of the force sensor based on a microfiber Bragg [146].

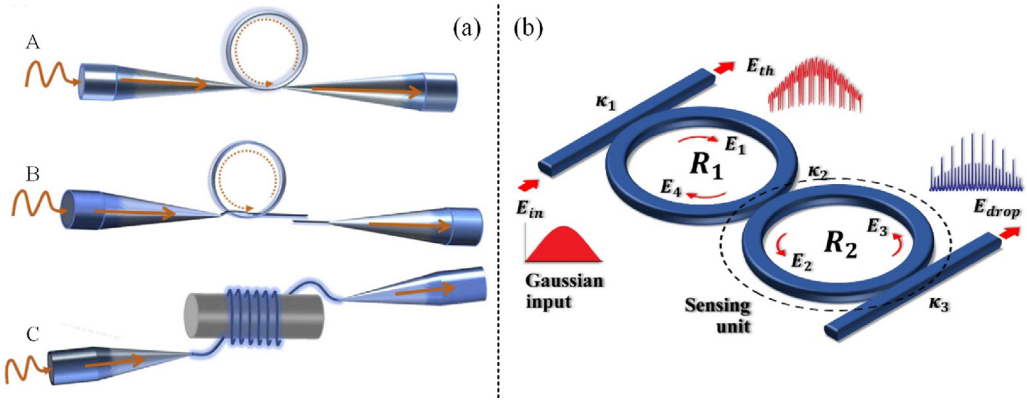

Fig. 18. (a) Schematic of MNF homogeneous MLR, MKR and MCR [148], (b) schematic diagram of the ring resonator system [152].

resonators and interferometers are particularly useful for sensing applications [148]. MNF resonators are divided into three types: microfibre loop resonator (MLR), microfibre knot resonator (MKR) and microfibre coil resonator (MCR). All those connection points couple via the strong evanescent field. MLR is formed by coiling the microfibre region to make a ring with two attached surfaces; MKR is formed by bending the microfibre to make a knot, and MCR is the basic functional element of microfibre photonics and is fabricated by winding a long microfibre on a cylinder with a low refractive index polymer coating [149]. The structure of MKR has a stronger coupling region and higher losses compared with the MLR, while the MCR is hardly used as a force sensor for its complicated structure. In 2005, MLR-based force sensor was presented with a sensitivity of 0.32 pm/$\mu\epsilon$ at the wavelength of 1310 nm.

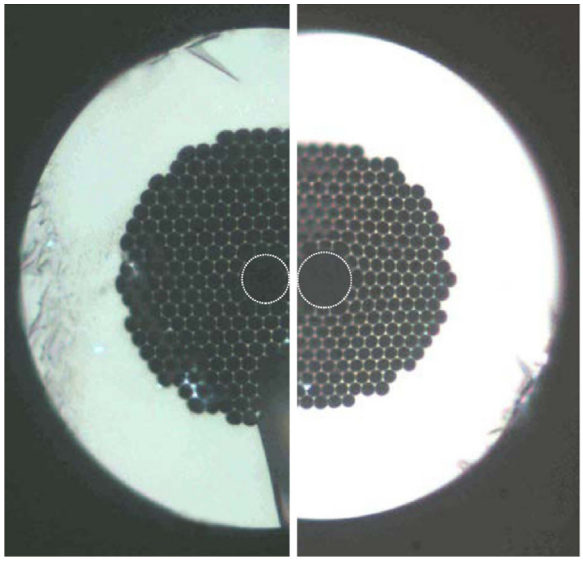

Fig. 19. Optical microscopy images of HC fiber cross-section before and after Electode Arc Discharge procedure [155].

The strain applied deforms the loop structure and finally results in the wavelength drift [150]. In 2014, a compact highly sensitive microfibre coupler-based reflective micro-force sensor was presented by forming a Sagnac loop. The force sensitivity was as high as 3754 nm/N, and the low detection limit was 1.6 μN [151]. In 2018, an optical double-ring resonator sensing system was presented to detect micronewton measurement-sensing devices based on optical sensors [152] (Fig. 18).

In addition, an axial force sensor was presented based on force-induced spectral shift as a result of diameter variation under axial force. The microfibre used in the sensor was tapered from a standard optical fibre showing an obvious sinusoidal oscillatory transmission spectrum due to the multimode interference. The strain sensitivity was 4.84 pm/με and the force detection limit was down to 50 μN with the microfibre diameter of 2.5 μm [153].

3.1.5. Sensors based on micro-structured optical fibres

Micro-structured optical fibres (MOFs) are a new kind of optical fibre that appeared in the last decade. The main difference between MOFs and regular optical fibres is that MOFs are made of a homogeneous medium, and the cladding is the fabricated air holes at the wavelength scale that are periodically distributed in the surroundings. The core of MOF is a defect that destroys the periodicity of the refractive index modulation by lacking one or more air holes in the centre. According to its transmission mechanism, MOFs can be divided into two categories, including the photonic bandgap MOF and the total internal reflective MOF, of which the former is more suitable for force sensing.

Similar to MNFs, MOFs are also integrated with FBG or microcavities for sensing. In 2013, a long-period grating fabricated in polymer micro-structured fibre for sensing was presented with the strain sensitivity of −1.39 pm/με, showing a linear response for the strain range up to 16.8 mε [154]. In 2014, long-period gratings were fabricated in hollow-core air-silica photonic bandgap fibres, and the axial strain sensitivity related to the resonant wavelength shift was calculated to be −139.16 pm/N [155,156]. In 2017, grapefruit-shaped micro-structured optical fibre Bragg gratings were made to be an optical fibre shear sensor. The sensitivity was defined as the ratio of notch visibility changes and shear force, which in turn was calculated to be 0.78 dB/N [157] (Figs. 19 and 20).

In 2010, the strain sensor realized by a photonic-crystal-fibre-based Sagnac loop was presented, whose sensitivity was −0.457 pm/N [158]. In the same year, a highly birefringent photonic crystal fibre was used as the sensing element inserted in a fibre loop mirror (FLM) to form a temperature-insensitive strain sensor. The output power of the strain sensor was only affected by the transmission spectral change of the FLM caused by the strain applied to the fibre with the sensitivity of 1.1 pm/N [159]. In 2012, an all-fibre optical Fabry-Perot interferometer strain sensor whose cavity was a microscopic air bubble was demonstrated with a strain sensitivity of 4 pm/N and a low-temperature sensitivity less than 0.9 pm/°C [160]. The strain sensor has the same working principle as those FPI strain sensors with an air bubble inside as mentioned before, and only differs in the fibre structure. A modified photonic crystal fibre-based Mach-Zehnder interferometer (PCF-MZI) strain sensor was also proposed by introducing a collapsed region to the middle of a normal PCF-MZI. The photonic crystal fibre-based sensors have extremely low thermal dependence, with a strain sensitivity of 11.22 dB/mε [161]. Additionally, a sensor based on a liquid-infiltrated micro-structured optical fibre was constructed by selective liquid infiltration of one particular cladding air hole in the MOF. Both theoretical analysis and experimental results indicated that the multiple-resonance peaks presented in the transmission spectrum possess different temperature and force sensitivities. The highest force sensitivity was 4.121 ± 0.197 nm/N, which could be roughly converted into the strain sensitivity of 3.769 ± 0.180 pm/με [162] (Fig. 21).

3.2. Other optical micro-force sensors

In addition to the frequently used optical fibre-based sensing methods above, some unique methods were used. In 1998, a force sensor using optical beam deflection (ODB) techniques for characterizing object interactions at the microscale was developed, which is used for AFM now. The cantilever deflection was detected by measuring the amount of a laser spot deflected via a quadrature photodiode. When a force is applied to the cantilever, the deformation of the cantilever leads to the deviation of the reflected spot, causing a deflected laser amount of variation [163] (Fig. 22).

In 2004, a micro-grating based force sensor integrated with a surface micromachined silicon-nitride probe was proposed. The optical-encoder force sensor can measure micronewton-scale force in the axial direction of the probe by sensing the axial deflections. It consists of two identical constant-period transmission phase gratings that are vertically aligned when no force is applied; when a force is applied to the axial direction of the probe, the upper index grating is displaced with respect to the bottom grating. This effect changed the diffraction efficiency of the phase grating; thus, the relative position of the two gratings can be determined by the intensities in the diffraction orders [164,165].

In 2018, a multiaxial tactile sensor was presented in order to realize the control of the gripping force by attaching the sensor on the manipulator. As the sensor approached the target object, a portion of the light was shielded, causing the light intensity to change. The proximity can be detected as the impedance change of the monocrystalline Si substrate by the reflected light from the object due to the photoconductive effect that formed photo-carriers [166] (Figs. 23 and 24).

In addition, as the micro-scale 3D printing technique named two-photon polymerization developed and commercialized over the past decade, micro-scale 3-dimensional structures can be easily fabricated. Researchers from the Imperial College of London presented a 3D compliant grasper with an integrated force sensor, the entirety of which was fabricated on the tip of an optical fibre in a single-step process using this fabrication method. The force estimation principle was optical interferometry, and achieved a force resolution of 0.05 μN [167]. The authors also designed a micro-scale fibre-optic force sensor made of a series of thin

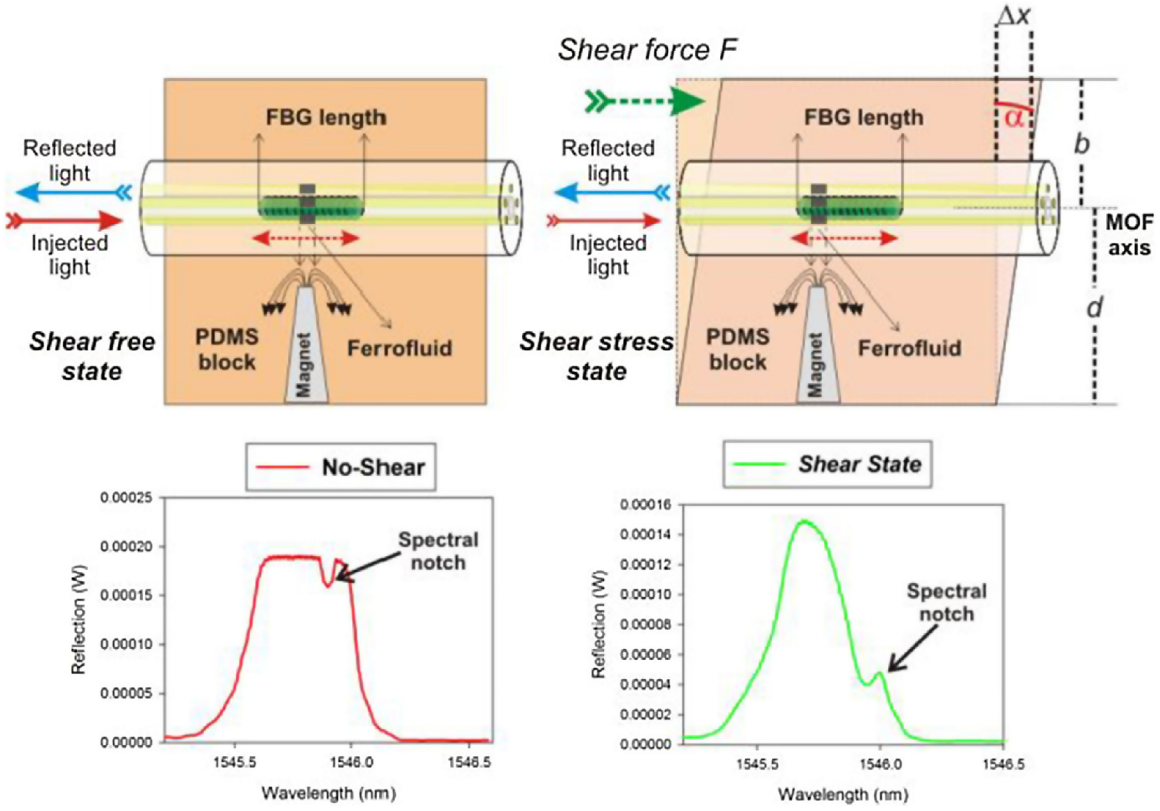

Fig. 20. Schematic representation of the operation principle of the shear sensor [157].

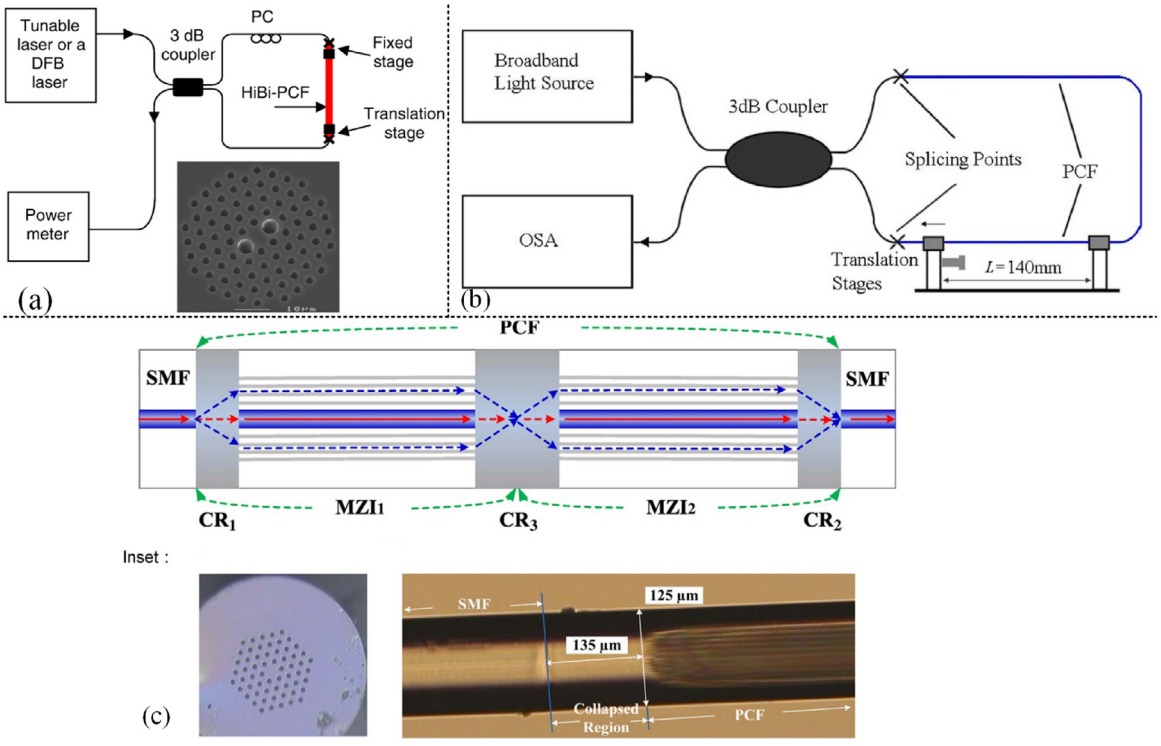

Fig. 21. (a) Experimental setup of the stain sensor based on PCF FLM [159], (b) experimental setup of the strain snesor using PCF-based Sagnac loop [158], (c) image of the modified PCF-MZI [161].

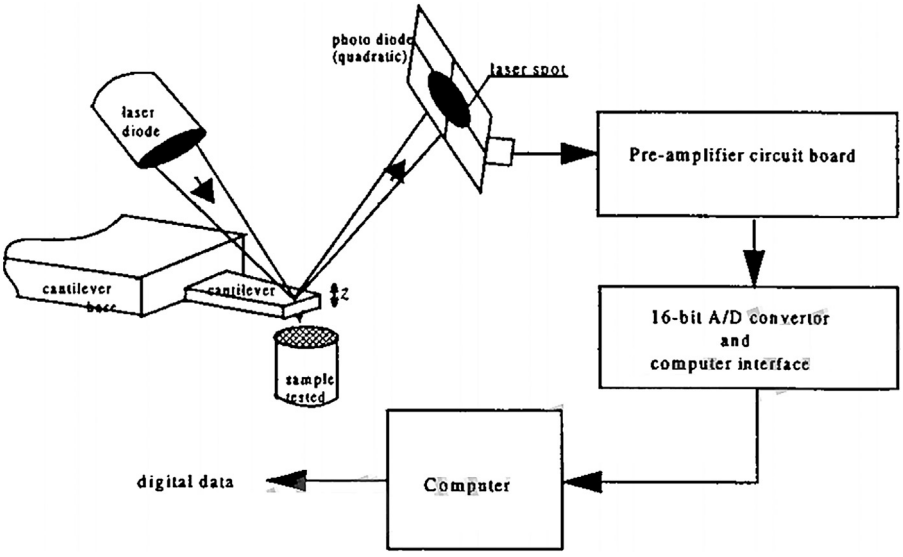

Fig. 22. The OBD force sensing system [163].

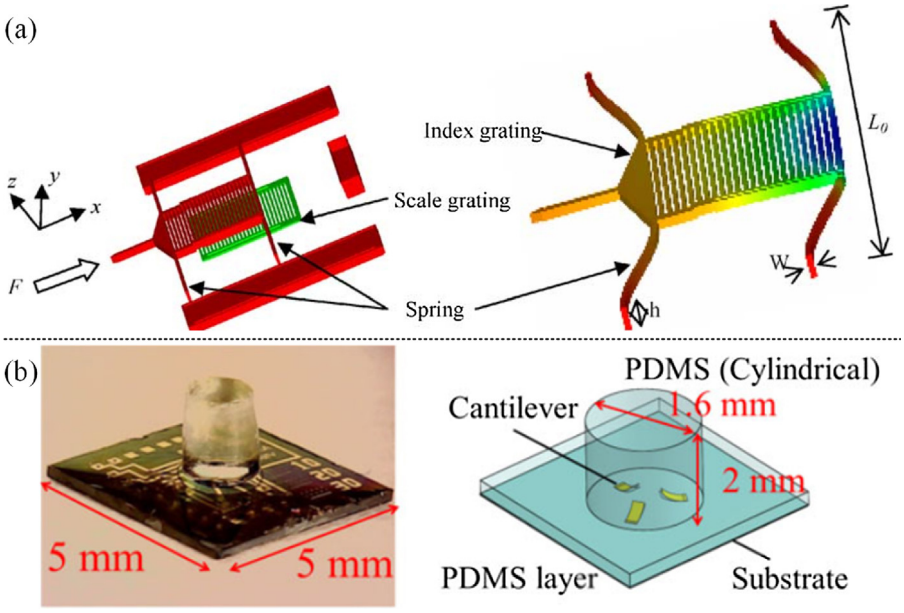

Fig. 23. (a) Solid model for optical-encoder force sensor [164],(b) the photograph and schematic illustration of the MEMSS sensor [166].

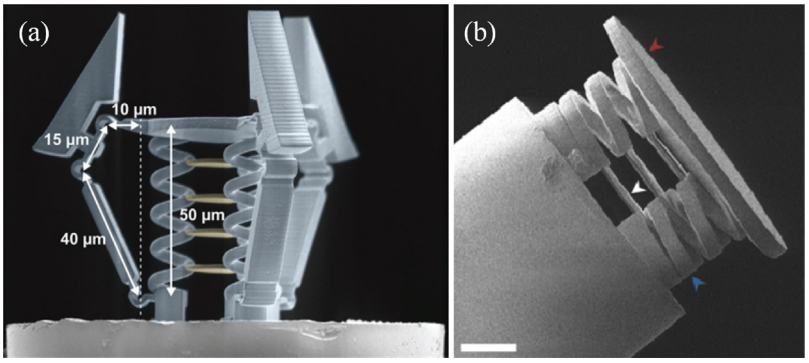

Fig. 24. (a) SEM image of gripper fabricated on the tip of an optical fiber by 2-photon polymerization [167], (b) SEM image of an optical FP force sensor fabricated by 2-photon polymerization [168].

plates, which were supported by springs that compress under an applied force. The interferometric changes at the proximal end of the fibre were read out using reflectance spectroscopy as the sensor was compressed. As a result, the resulting spectral changes were calibrated with respect to the applied force. The proof-of-concept force sensing was demonstrated to be over the range of 0-50 μN, with a measurement error of approximately 1.5 μN [168].

3.3. Vision-based micro-force sensing method

All the fibre sensing methods referred to above are rarely used in micromanipulation system currently because the technology is not mature enough and the measuring equipment is complex. Instead, the vision-based micro-force sensing method that is carried out by measuring the deformation or displacement of a structure by vision is more widely used.

Li et al. devised a method for micro-motion detection of a 3-DOF precision positioning stage [169] and then established a micro-vision imaging system to track in-plane displacements with nanometric accuracy [170]. Wu [171] and Zhang et al. [172,173] developed a robust rotation-invariant displacement measurement method for the micro/nano-positioning system with a theoretical accuracy of 0.01 pixel. This technique allows the measurement of static forces with a very high resolution and does not require an external field, such as thermal and electrical fields. Vision-based sensing technology even has the ability to work in aqueous medium, which makes it more suitable for force sensing in the cell manipulation process.

Early in 2006, Giouroudi et al. used two CCD cameras for actual axis positions measurement of the end-effector to realize force feedback [174]. In 2010, miniature grippers with vision-based force sensing were designed for manipulation of zebrafish egg cells less than 1 mm in diameter. The manipulation forces were obtained from known information in other areas and estimated to be approximately 10 mN [175]. In 2012, an automated nanomanipulation with a parallel imaging/manipulation force microscope was presented with one cantilever acting as an imaging sensor and the other as a manipulating tool [176]. In 2017, a vision-based sensing method was used to characterize the force at a CNT/Au side-contact interface inside a scanning electron microscope (SEM). The AFM cantilever was used in the SEM measuring system as the sensing element. By monitoring the deformation of the cantilever, a contact force as small as several hundreds of nanonewtons can be obtained [177]. In 2018, a microgripper with two degrees of freedom for the manipulation of micro-objects was designed, integrated with image process technology using LabVIEW tools for gripping force measurement [77]. All these systems discussed above obtained force information by monitoring the deformation of end-effectors. However, monitoring that of the operated objects such as the cells can also be used for force analysis. Fatemeh Karimirad et al. put forward a vision-based measurement method using an artificial neural network model to measure the applied load to a spherical biological cell during the micromanipulation process. The measurement was achieved by obtaining the cell contour image first and then determining the deformation region angle of the cells [178,179] (Fig. 25).

4. Discussion

This section compares the parameters of different kinds of sensors and then summarizes the frequently used fabrication methods briefly.

4.1. Results of parameter comparison

At first, several typical works on the micro-force sensors arranged by chronological order is presented in fig. 26.

The resolution and sensitivity are compared among five types of electrical micro-force sensors in Table 1. The parameters of optical force sensors are discussed mainly regarding their resolution, force sensitivity and temperature sensitivity in Tables 2 and 3.

It can be known from Table 1 that the resolution of the capacitive type force sensor is the highest but that of the strain gauge-based sensors is relatively low. The piezoresistive type of sensor is slightly better than the piezoelectric type of sensor. Although the piezoresistive principle is the main principle of the strain gauge, they are mostly used for rough measurement. The capacitive type of force sensor is the most used one for integrating with the micromanipulation system end-effector, followed by the piezoresistive type. However, the limitations of processing technology restrain the performance of capacitive force sensors. The combs defect easily, and the size is limited.

Table 2 demonstrates the resolution of some optical force fibre sensors. The optical force sensors have not been widely used in micro-scale force measurement. Most are for conventional macro-scale applications, such as underground mines and rock cracking; some recent research is aimed at smaller scales but not the micro-scale, such as the robot and minimally invasive surgery operating equipment. As a result, the resolution is not higher than that of the electrical micro-force sensors. The optical fibre sensors are always used as strain sensors, and the resolution is also expressed as strain value because the parameters of optical fibre change along with the deformation of the fibre itself.

Table 3 shows the parameter comparison of different kinds of optical fibre sensors. As optical fibres are sensitive to the environmental variation, the environment temperature variation also shows the output signal change. In this section, temperature-induced force measurement error was put forward to evaluate the relative temperature sensitivity of force sensors. The larger the temperature-induced force measurement error is, the more susceptible to the temperature the force sensor is. According to the parameter comparison, the FPI type of sensor is more sensitive to force and less susceptible to temperature than the FBG type. The less used MZI type and optical energy change type of force sensor have regular force sensitivity, but the latter is hardly susceptible to temperature. In addition, the MNF type of sensor has rather high force sensitivity but is barely resistant to temperature. The MOF type of sensor performs moderately, but the refractive index distribution of the fibre can be freely designed. In conclusion, the FBG and FPI types of sensors are the most commonly used to date, among which the FPI type performs better.

Compared with electrical micro-force sensors, most of the optical fibre sensors measure force by the variation in light wavelength, which is realized by adopting a spectrograph with a few tenths of a nanometre or even several picometre resolutions. Furthermore, the size of optical sensing elements is small. Optical fibres are the basic sensing elements of optical fibre sensors. The diameter of single-mode fibre is one hundred microns, while that of micro-nano fibre is down to several microns or a few hundred nanometres. The two-photon polymerization can even fabricate micro-grippers on the cross section of single-mode fibres. The vision-based micro-force sensing method measures without parts placed inside the micro-operating system. All these examples illustrate the small size of optical force sensing methods.

4.2. Summary of fabrication methods

Microfabrication techniques, the primary means of manufacturing microelectro-mechanical systems, developed from the

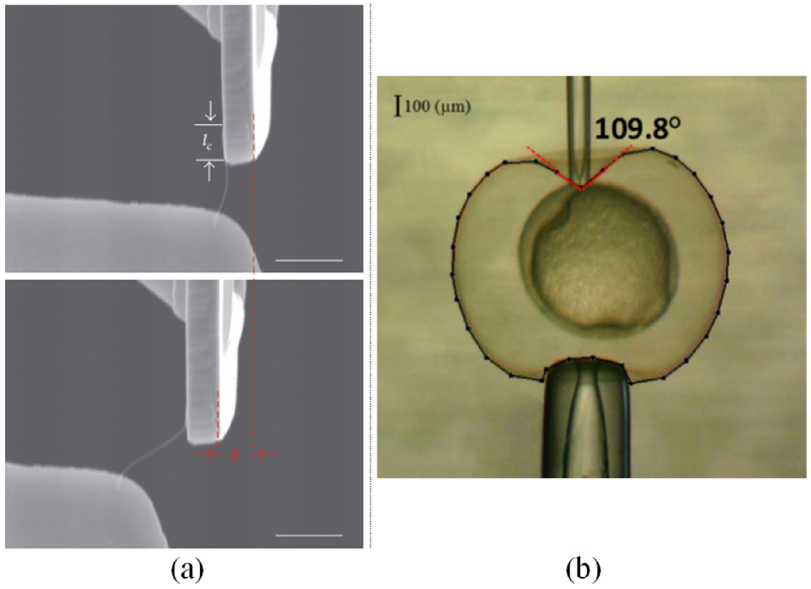

Fig. 25. (a) Vander Waals force measurement at the CNT/Au interface [177], (b) force measurement utilizing the defromation of cell [178].

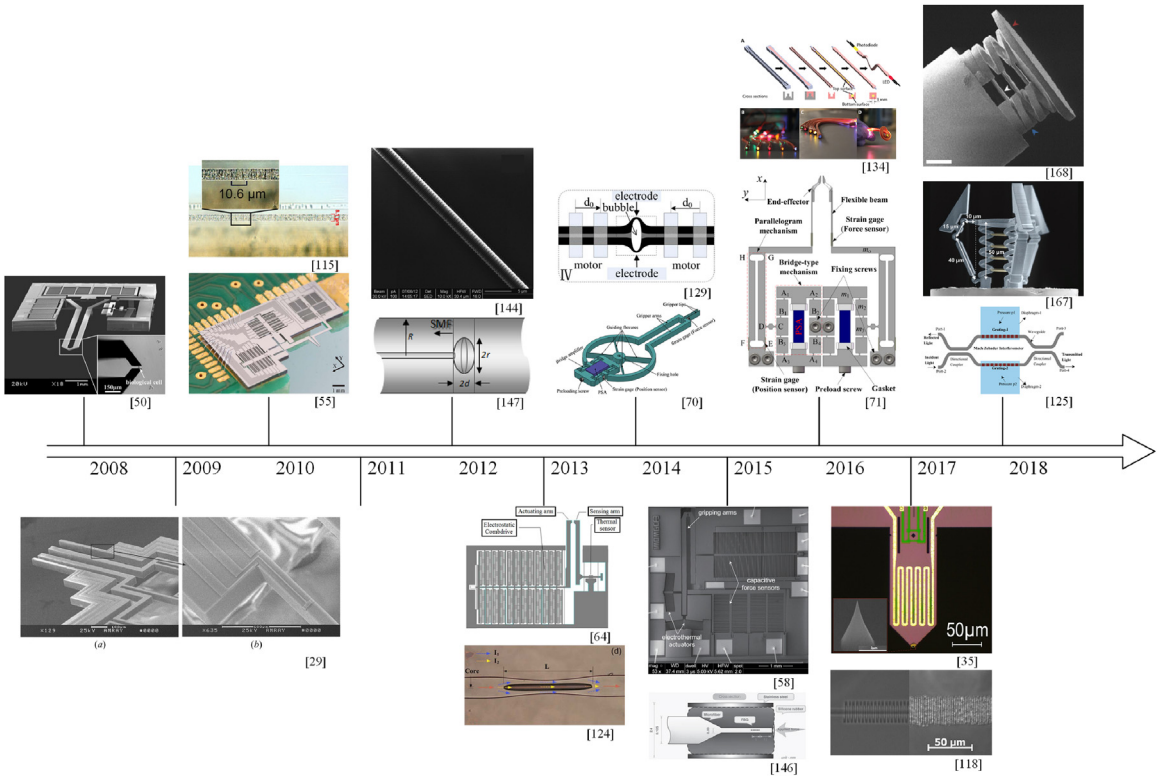

Fig. 26. Typical works about the micro-force sensors.

manufacturing technology of the integrated circuit (IC). These approaches mainly include surface micromachining technology, such as photoetching and chemical vapour deposition (CVD); bulk micromachining technology, such as focus ion-beam-etching (FIB), isotropy and anisotropic etching; super-precision machine processing technology, such as stereo lithography appearance (SLA) and micro electrical discharge machining (micro EDM); and the LIGA technique is realized by the photolithography, galvanoformung and deforming of X-rays.

In Section 5, most sensors are integrated with micro-grippers forming the microelectro-mechanical system, and they are fabricated by the above methods. Surface and bulk micromachining fabrication technologies are used to fabricate microgrippers from silicon wafers in reference [29]; the piezoresistors in [32] are defined using reactive ion etching (RIE); and the microgrippers in [50] are fabricated with a silicon-on-insulator (SOI) wafer related to chemical vapour deposition, reactive ion etching and wet etch methods.

Those optical sensors, including FBGs, air cavities inside fibres, micro-nano fibres and micro-structured optical fibre, are not typical MEMS elements. All of them have specific fabrication methods, and the following content provides an introduction.

Table 1
Parameter comparison of electrical micro-force sensors.

Type	Resolution	Sensitivity	Supplementary	Examples	Year
Piezoresistive type	3 μN	72 V/N		[29,30]	2009
	4 μN, 21 μN	540 V/N, 100 V/N	2-dimensional	[32,33]	2012
	1 μN, 20 μN	2.8 V/N	Local and global	[34]	2013
Piezoelectric type	14.5 μN			[40]	2006
	Sub-micronewton (μN)	190.1 V/N		[42]	2009
	800 μN	1.23 V/N		[46,47]	2017
Capacitive type	19.9 nN, 38.5 nN		Contact and gripping force	[50–54]	2009
	60 nN			[55]	2010
Electrothermal type		1.25 N/m		[64]	2013
		5.58×10^4 V/N		[65]	2014
Strain gauge	143 mN			[69]	2013
		658.345 V/N		[70]	2014
	0.035 mN			[71]	2016
	0.31 mN, 20.51 mN	3.34×10^{-2} V/N, 1.6×10^{-4} V/N	double precision	[72]	2017
	0.05 mN	14.204 V/N		[73]	2017

Table 2
Resolution of some optical force sensors.

Type	Resolution	Supplementary	Examples	Year
FBG	0.5 με		[102]	2010
	1 με		[103]	2016
	10 με		[104]	2015
	4.6 mN		[109]	2018
	1.85 mN, 0.074 mN	Axial and radial	[112,113]	2018
	30 με		[115]	2010
	8 mN, 4 mN	Axial and radial	[116,117]	2013
MNF	1.6 με		[151]	2014

Table 3
Parameter comparison of electrical micro-force sensors.

Type	Force sensitivity	Temperature sensitivity	Temperatured-induced force measurement error	Examples	Year
FBG	6.2 pm/με			[106]	2018
	1.13 pm/με	−50.1 pm/°C	−44.340 με/°C	[115]	2010
	8.3 pm/MPa, 4.16 pm/MPa	11.6 pm/°C	1.398 MPa/°C, 2.788 MPa/°C	[118]	2017
	1.2 pm/με	10 pm/°C	8.330 με/°C	[119]	2018
MZI	6.8 pm/με			[124]	2013
	0.2 pm/MPa			[125]	2018
FPI	30.66 pm/με	1.2 pm/°C	0.039 με/°C	[126]	2014
	10.3 pm/με	0.95 pm/°C	0.092 με/°C	[127]	2012
	1.2 pm/με	11.7 pm/°C	9.750 με/°C	[128]	2014
	6.0 pm/με	1.1 pm/°C	0.183 με/°C	[129]	2014
	43.0 pm/με	2.0 pm/°C	0.047 με/°C	[130]	2015
	8.11 pm/N	200 pm/°C	24.660 N/°C	[131]	2013
Optical energy change	0.126 dB/N, 0.015 dB/N			[135]	2018
	0.26 μs/με	0.01 μs/°C	0.038 με/°C	[138]	2017
MNF	6.38 pm/με	14 pm/°C	2.194 με/°C	[147]	2015
	3.754×10^6 pm/N			[151]	2014
	4.84 pm/με			[153]	2014
MOF	−139.16 pm/N			[155,156]	2014
	0.78 dB/N			[157]	2017
	4 pm/N	0.9 pm/°C	0.225 N/°C	[160]	2012
	3.769 pm/με			[162]	2014

The gratings inside FBGs were induced based on photosensitivity using the phase mask technique and point-by-point technique with a CO2 laser, electric arc and ultraviolet laser in early years [154,180], but the photosensitivity for a specific wavelength and material limited the utilization. A femtosecond pulsed laser can fabricate gratings inside FBGs without utilizing the photosensitivity, but its high energy density changes the refractive index [121]. Some FBGs based on micro-fibres tapered from standard non-photosensitive single-mode fiber are inscribed by a focused-ion-beam machining method, causing periodic variation of the diameter [144].

The air cavities inside fibres are created by means of splicing together two sections of standard single-mode fibres, accompanying easy pretreatment on the fibre ends, forming in-fibre Fabry-Perot interferometers [129]. The two-step drawing process was presented by researchers for fabricating long uniform micro-nano fibres by a flame-heated fibre drawing method [140].The micro-structured optical fibres have the same pulling process but with controlled inert gas pressure and speed to form the micro-structure. The structure referred to in [167,168] used the 2-photon polymerization method, permitting versatile maskless 3D-printing of microscale structures with features as small as 100 nm.

The fabrication methods of small scale sensors are multifarious, and some new technology will be put forward in the near future.

5. Conclusion

In a micro/nano manipulation system, force sensing is required to prevent from sample damage. The mechanical property measured by a force sensor is an important parameter for samples as well. The structures inside the micro/nano manipulation system are compact, restricting the manipulation space of the system, so it is better to utilize a non-contact micro-force sensor. One way to achieve this goal is by integrating sensors on manipulation end-effectors, which prevents direct contact between samples and sensors. To measure the micro force effectively, the micro-force sensors suitable for micro/nano manipulation systems need to possess small size, high sensitivity, high resolution and interference immunity ability.

Section 2 introduced several kinds of commonly used electrical micro-force sensors. According to the comparison result, the capacitive type of sensors has a rather high resolution, which can measure dozens of nanonewtons. The capacitive type of sensor is the most commonly used type, and next is the piezoresistive type for its simple structure, while the size of the capacitive sensor is restricted for the processing technique.

Section 3 provided a presentation about optical force sensors. FBG-based sensors have more mature processing technology than other optical fibre sensors, but the sensitivity and anti-temperature-interference ability is weaker than that of FPI-based force sensors. Micro/nano fibre has a smaller diameter that is down to several micrometres and has higher sensitivity. The parameters of microstructured optical fibre are not the best but the refractive index distribution can be artificially designed. The visual-based sensing method is another common method in micro-force sensing.

Integrated circuits tend to be replaced by integrated optical circuits for their high speed and low loss properties in the transmission procedure and their ability to resist electromagnetic interference. The small size and high resolution also impel the wide application of optical fibres for sensing. As a result, the optical fibre-based sensing methods and other optical sensing methods such as visual-based methods and those utilizing optical theory without optical fibres have been developing for years. Although the optical force sensing methods have many advantages, research on the utilization of them in micro/nanometre manipulation systems is scant because many optical fibre sensors are focused on the measurement of the refractive index or gas, and most fibre force sensors are concentrated on macro-scale force sensing applications such as robot hand fingers and minimally invasive surgery. Therefore, optical sensing methods, especially optical fibre-based force sensors, show potential for their utilization in micro/nano manipulation systems and can be paid more attention in the research field.

Acknowledgement

This work is supported by the National Natural Science Foundation of China (Grant No. 51820105007) and the Pearl River Nova Program of Guangzhou (201906010061). These supports are greatly appreciated.

References

[1] H. Xie, S. Régnier, Three-dimensional automated micromanipulation using a nanotip gripper with multi-feedback, J. Micromech. Microeng. 19 (7) (2009) 075009.
[2] M. Jiang, G. Wang, W. Xu, W. Ji, N. Zou, H.P. Ho, X. Zhang, Two-dimensional arbitrary nano-manipulation on a plasmonic metasurface, Optics Lett. 43 (7) (2018) 1602–1605.
[3] P. Pan, W. Wang, C. Ru, Y. Sun, X. Liu, MEMS-based platforms for mechanical manipulation and characterization of cells, J. Micromech. Microeng. 27 (12) (2017) 123003.
[4] X. Liu, Y. Sun, W. Wang, B.M. Lansdorp, Vision-based cellular force measurement using an elastic microfabricated device, J. Micromech. Microeng. 17 (7) (2007) 1281.
[5] E. Moeendarbary, A.R. Harris, Cell mechanics: principles, practices, and prospects, Wiley Interdiscip. Rev. Syst. Biol. Med. 6 (5) (2014) 371–388.
[6] Y. Sun, K.T. Wan, K.P. Roberts, J.C. Bischof, B.J. Nelson, Mechanical property characterization of mouse zona pellucida, IEEE Trans. Nanobiosci. 2 (4) (2003) 279–286.
[7] A. Tibrewala, A. Phataralaoha, S. Büttgenbach, Simulation, fabrication and characterization of a 3D piezoresistive force sensor, Sens. Actuators A: Phys. 147 (2) (2008) 430–435.
[8] A. Sieber, P. Valdastri, K. Houston, C. Eder, O. Tonet, A. Menciassi, P. Dario, A novel haptic platform for real time bilateral biomanipulation with a MEMS sensor for triaxial force feedback, Sens. Actuators A: Phys. 142 (1) (2008) 19–27.
[9] M. Garcés-Schröder, D. Metz, M. Leester-Schädel, A. Dietzel, Micromechanical systems for the mechanical characterization of muscle tissue, Proc. Eng. 120 (2015) 849–852.
[10] L. Wang, W. Dou, M. Malhi, M. Zhu, H. Liu, J. Plakhotnik, Z. Xu, Q. Zhao, J. Chen, S. Chen, et al., Microdevice platform for continuous measurement of contractility, beating rate, and beating rhythm of human-induced pluripotent stem cell-cardiomyocytes inside a controlled incubator environment, ACS Appl. Mater. Interfaces 10 (25) (2018) 21173–21183.
[11] Y.R. Wang, J.M. Zheng, G.Y. Ren, P.H. Zhang, C. Xu, A flexible piezoelectric force sensor based on PVDF fabrics, Smart Mater. Struct. 20 (4) (2011) 045009.
[12] Y. Xie, D. Sun, H.Y.G. Tse, C. Liu, S.H. Cheng, Force sensing and manipulation strategy in robot-assisted microinjection on zebrafish embryos, IEEE/ASME Trans. Mechatron. 16 (6) (2011) 1002–1010.
[13] F. Beyeler, S. Muntwyler, B.J. Nelson, A six-axis MEMS force-torque sensor with micro-newton and nano-newtonmeter resolution, J. Microelectromech. Syst. 18 (2) (2009) 433–441.
[14] M. Bulut Coskun, S. Moore, S.R. Moheimani, A. Neild, T. Alan, Zero displacement microelectromechanical force sensor using feedback control, Appl. Phys. Lett. 104 (15) (2014) 153502.
[15] J. Rajagopalan, A. Tofangchi, M.T.A. Saif, Linear high-resolution bioMEMS force sensors with large measurement range, J. Microelectromech. Syst. 19 (6) (2010) 1380–1389.
[16] S. Yang, Q. Xu, A review on actuation and sensing techniques for MEMS-based microgrippers, J. Micro-Bio Robot. 13 (1) (2017) 1–14.
[17] W. Chen, X. Zhang, S. Fatikow, A novel microgripper hybrid driven by a piezoelectric stack actuator and piezoelectric cantilever actuators, Rev. Sci. Instrum. 87 (11) (2016) 115003.
[18] W. Chen, X. Zhang, S. Fatikow, Design, modeling and test of a novel compliant orthogonal displacement amplification mechanism for the compact micro-grasping system, Microsyst. Technol. 23 (7) (2017) 2485–2498.
[19] W. Chen, X. Zhang, H. Li, J. Wei, S. Fatikow, Nonlinear analysis and optimal design of a novel piezoelectric-driven compliant microgripper, Mech. Mach. Theory 118 (2017) 32–52.
[20] X. Sun, W. Chen, S. Fatikow, Y. Tian, R. Zhou, J. Zhang, M. Mikczinski, A novel piezo-driven microgripper with a large jaw displacement, Microsyst. Technol. 21 (4) (2015) 931–942.
[21] K.N. Andersen, D. Petersen, K. Carlson, K. Mølhave, O. Sardan, A. Horsewell, V. Eichhorn, S. Fatikow, P. Bøggild, Multimodal electrothermal silicon microgrippers for nanotube manipulation, IEEE Trans. Nanotechnol. 8 (1) (2009) 76–85.
[22] B.K. Chen, Y. Zhang, D.D. Perovic, Y. Sun, MEMS microgrippers with thin gripping tips, J. Micromech. Microeng. 21 (10) (2011) 105004.
[23] G. Perret, T. Lacornerie, F. Manca, S. Giordano, M. Kumemura, N. Lafitte, L. Jalabert, M.C. Tarhan, E.F. Lartigau, F. Cleri, Real-time mechanical characterization of DNA degradation under therapeutic X-rays and its theoretical modeling, Microsyst. Nanoeng. 2 (2016) 16062.
[24] P. Liu, L. Dong, F. Arai, T. Fukuda, Nanotube multi-functional nanoposition sensors, Proc. Inst. Mech. Eng. Part N: J. Nanoeng. Nanosyst. 219 (1) (2005) 23–27.
[25] V. Eichhorn, M. Bartenwerfer, S. Fatikow, Nanorobotic assembly and focused ion beam processing of nanotube-enhanced AFM probes, IEEE Trans. Autom. Sci. Eng. 9 (4) (2012) 679–686.
[26] G. Meyer, N.M. Amer, Novel optical approach to atomic force microscopy, Appl. Phys. Lett. 53 (12) (1988) 1045–1047.
[27] M. Tortonese, R.C. Barrett, C.F. Quate, Atomic resolution with an atomic force microscope using piezoresistive detection, Appl. Phys. Lett. 62 (8) (1998) 834–836.
[28] A.A. Barlian, W.T. Park, J.R. Mallon, A.J. Rastegar, B.L. Pruitt, Semiconductor piezoresistance for microsystems, Proc. IEEE 97 (3) (2009) 513–552.
[29] T. Chen, L. Chen, L. Sun, X. Li, Design and fabrication of a four-arm-structure MEMS gripper, IEEE Trans. Ind. Electron. 56 (4) (2009) 996–1004.
[30] T. Chen, L. Chen, L. Sun, Piezoelectrically driven silicon microgrippers integrated with sidewall piezoresistive sensor, 2009 IEEE International Conference on Robotics and Automation (2009) 2989–2994, IEEE.
[31] T.C. Duc, G.K. Lau, J.F. Creemer, P.M. Sarro, Electrothermal microgripper with large jaw displacement and integrated force sensors, J. Microelectromech. Syst. 17 (6) (2008) 1546–1555.
[32] T.C. Duc, J.F. Creemer, P.M. Sarro, Piezoresistive cantilever beam for force sensing in two dimensions, IEEE Sens. J. 7 (1) (2006) 96–104.

[33] A.A. Abbasi, M.T. Ahmadian, Force controlled manipulation of biological cells using a monolithic MEMS based nano-micro gripper, ASME 2012 International Mechanical Engineering Congress and Exposition (2012) 193–201, American Society of Mechanical Engineers.
[34] J. Wei, M. Porta, M. Tichem, U. Staufer, P.M. Sarro, Integrated piezoresistive force and position detection sensors for micro-handling applications, J. Microelectromech. Syst. 22 (6) (2013) 1310–1326.
[35] A. Sierakowski, D. Kopiec, W. Majstrzyk, P. Kunicki, P. Janus, R. Dobrowolski, P. Grabiec, I.W. Rangelow, T. Gotszalk, Magnetoelectric versus thermal actuation characteristics of shear force AFM probes with piezoresistive detection, Meas. Sci. Technol. 28 (3) (2017) 034011.
[36] W. Majstrzyk, A. Ahmad, T. Ivanov, A. Reum, T. Angelow, M. Holz, T. Gotszalk, I. Rangelow, Thermomechanically and electromagnetically actuated piezoresistive cantilevers for fast-scanning probe microscopy investigations, Sens. Actuators A: Phys. 276 (2018) 237–245.
[37] Y. Wei, Q. Xu, An overview of micro-force sensing techniques, Sens. Actuators A: Phys. 234 (2015) 359–374.
[38] R. Zeng, K.W. Kwok, H.L.W. Chan, C.L. Choy, Longitudinal and transverse piezoelectric coefficients of lead zirconate titanate/vinylidene fluoride-trifluoroethylene composites with different polarization states, J. Appl. Phys. 92 (5) (2002) 2674–2679.
[39] Y. Shen, N. Xi, K.W. Lai, W.J. Li, A novel pvdf microforce/force rate sensor for practical applications in micromanipulation, Sens. Rev. 24 (3) (2004) 274–283.
[40] D.H. Kim, C.N. Hwang, Y. Sun, S.H. Lee, B. Kim, B.J. Nelson, Mechanical analysis of chorion softening in prehatching stages of zebrafish embryos, IEEE Trans. Nanobiosci. 5 (2) (2006) 89–94.
[41] Z. Chen, K.-Y. Kwon, X. Tan, Integrated ipmc/pvdf sensory actuator and its validation in feedback control, Sens. Actuators A: Phys. 144 (2) (2008) 231–241.
[42] H.B. Huang, D. Sun, J.K. Mills, S.H. Cheng, Robotic cell injection system with position and force control: toward automatic batch biomanipulation, IEEE Trans. Robot. 25 (3) (2009) 727–737.
[43] G. Wang, Q. Xu, Design and precision position/force control of a piezo-driven microinjection system, IEEE/ASME Trans. Mechatron. 22 (4) (2017) 1744–1754.
[44] Y. Wei, Q. Xu, Design of a PVDF-MFC force sensor for robot-assisted single cell microinjection, IEEE Sens. J. 17 (13) (2017) 3975–3982.
[45] A.H. Korayem, M.H. Korayem, The effect of surface roughness on the vibration behavior of AFM piezoelectric MC in the vicinity of sample surface in air environment based on MCS theory, Precis. Eng. 47 (2017) 212–222.
[46] A.H. Korayem, A. Mashhadian, M.H. Korayem, Vibration analysis of different afm cantilever with a piezoelectric layer in the vicinity of rough surfaces, Eur. J. Mech. – A/Solids 65 (2017) 313–323.
[47] M.H. Korayem, A.H. Korayem, Modeling of AFM with a piezoelectric layer based on the modified couple stress theory with geometric discontinuities, Appl. Math. Model. 45 (2017) 439–456.
[48] R. Schulze, T. Gessner, M. Heinrich, M. Schueller, R. Forke, D. Billep, M. Sborikas, M. Wegener, Integration of piezoelectric polymer transducers into microsystems for sensing applications, Proceedings of ISAF-ECAPD-PFM 2012 (2012) 1–4, IEEE.
[49] F. Beyeler, A. Neild, S. Oberti, D.J. Bell, Y. Sun, J. Dual, B.J. Nelson, Monolithically fabricated microgripper with integrated force sensor for manipulating microobjects and biological cells aligned in an ultrasonic field, J. Microelectromech. Syst. 16 (1) (2007) 7–15.
[50] K. Kim, X. Liu, Y. Zhang, Y. Sun, Nanonewton force-controlled manipulation of biological cells using a monolithic mems microgripper with two-axis force feedback, J. Micromech. Microeng. 18 (5) (2008) 055013.
[51] K. Kim, Y. Sun, R.M. Voyles, B.J. Nelson, Calibration of multi-axis MEMS force sensors using the shape-from-motion method, IEEE Sens. J. 7 (3) (2007) 344–351.
[52] X. Liu, K. Kim, Y. Zhang, Y. Sun, Nanonewton force sensing and control in microrobotic cell manipulation, Int. J. Robot. Res. 28 (8) (2009) 1065–1076.
[53] K. Kim, X. Liu, Y. Zhang, J. Cheng, X.Y. Wu, Y. Sun, Elastic and viscoelastic characterization of microcapsules for drug delivery using a force-feedback MEMS microgripper, Biomed. Microdevices 11 (2) (2009) 421–427.
[54] K. Kim, X. Liu, Y. Zhang, J. Cheng, X.Y. Wu, Y. Sun, Manipulation at the nanonewton level: micrograpsing for mechanical characterization of biomaterials, 2009 IEEE International Conference on Robotics and Automation (2009) 902–907, IEEE.
[55] S. Muntwyler, B.E. Kratochvil, F. Beyeler, B.J. Nelson, Monolithically integrated two-axis microtensile tester for the mechanical characterization of microscopic samples, J. Microelectromech. Syst. 19 (5) (2010) 1223–1233.
[56] Y. Jia, Q. Xu, Design of a monolithic dual-axis electrostatic actuation MEMS microgripper with capacitive position/force sensors, 2013 13th IEEE International Conference on Nanotechnology (IEEE-NANO 2013) (2013) 817–820, IEEE.
[57] Y. Jia, M. Jia, Q. Xu, A dual-axis electrostatically driven MEMS microgripper, Int. J. Adv. Robot. Syst. 11 (11) (2014) 187.
[58] J. Qu, W. Zhang, A. Jung, S. Silva-Da Cruz, X. Liu, A MEMS microgripper with two-axis actuators and force sensors for microscale mechanical characterization of soft materials, 2015 IEEE International Conference on Automation Science and Engineering (CASE) (2015) 1620–1625, IEEE.
[59] J. Qu, W. Zhang, A. Jung, S. Silva-Da Cruz, X. Liu, Microscale compression and shear testing of soft materials using an MEMS microgripper with two-axis actuators and force sensors, IEEE Trans. Autom. Sci. Eng. 14 (2) (2017) 834–843.
[60] Q. Xu, Design, fabrication, and testing of an MEMS microgripper with dual-axis force sensor, IEEE Sens. J. 15 (10) (2015) 6017–6026.
[61] S. Yang, Q. Xu, Z. Nan, Design and development of a dual-axis force sensing MEMS microgripper, J. Mech. Robot. 9 (6) (2017) 061011.
[62] S. Yang, Q. Xu, Design and analysis of a decoupled XY MEMS microgripper with integrated dual-axis actuation and force sensing, IFAC-PapersOnLine 50 (1) (2017) 808–813.
[63] D.M. Ştefănescu, M.A. Anghel, Electrical methods for force measurement – a brief survey, Measurement 46 (2) (2013) 949–959.
[64] B. Piriyanont, S.R. Moheimani, Design, modeling, and characterization of a MEMS micro-gripper with an integrated electrothermal force sensor, 2013 IEEE/ASME International Conference on Advanced Intelligent Mechatronics (2013) 348–353, IEEE.
[65] B. Piriyanont, S.R. Moheimani, MEMS rotary microgripper with integrated electrothermal force sensor, J. Microelectromech. Syst. 23 (6) (2014) 1249–1251.
[66] B. Piriyanont, A.G. Fowler, S.O.R. Moheimani, Force-controlled MEMS rotary microgripper, J. Microelectromech. Syst. 24 (4) (2015) 1164–1172.
[67] S. Yang, Q. Xu, Design of a microelectromechanical systems microgripper with integrated electrothermal actuator and force sensor, Int. J. Adv. Robot. Syst. 13 (5) (2016), 1729881416663375.
[68] W. Chen, X. Shi, W. Chen, J. Zhang, A two degree of freedom micro-gripper with grasping and rotating functions for optical fibers assembling, Rev. Sci. Instrum. 84 (11) (2013) 115111.
[69] D.H. Wang, Q. Yang, H.M. Dong, A monolithic compliant piezoelectric-driven microgripper: design, modeling, and testing, IEEE/ASME Trans. Mechatron. 18 (1) (2013) 138–147.
[70] Q. Xu, Design and smooth position/force switching control of a miniature gripper for automated microhandling, IEEE Trans. Ind. Inform. 10 (2) (2014) 1023–1032.
[71] Y.L. Yang, Y.D. Wei, J.Q. Lou, F.R. Xie, L. Fu, Development and precision position/force control of a new flexure-based microgripper, J. Micromech. Microeng. 26 (1) (2016) 015005.
[72] Q. Xu, Design and development of a novel compliant gripper with integrated position and grasping/interaction force sensing, IEEE Trans. Autom. Sci. Eng. 14 (3) (2017) 1415–1428.
[73] G. Wang, Q. Xu, Design and development of a piezo-driven microinjection system with force feedback, Adv. Robot. 31 (23–24) (2017) 1349–1359.
[74] K. Reck, N.S. Almind, M. Mar, J. Hübner, O. Hansen, E.V. Thomsen, Design and modeling of an all-optical frequency modulated MEMS strain sensor using nanoscale bragg gratings, SENSORS, 2009 IEEE (2009) 873–877, IEEE.
[75] J. Guo, M. Niu, C. Yang, Highly flexible and stretchable optical strain sensing for human motion detection, Optica 4 (10) (2017) 1285–1288.
[76] G. Fragiacomo, K. Reck, L. Lorenzen, E. Thomsen, Novel designs for application specific MEMS pressure sensors, Sensors 10 (11) (2010) 9541–9563.
[77] R.D. Dsouza, K.P. Navin, T. Theodoridis, P. Sharma, Design, fabrication and testing of a 2 DOF compliant flexural microgripper, Microsyst. Technol. 24 (9) (2018) 3867–3883.
[78] A.W. Snyder, J. Love, Optical Waveguide Theory, Springer Science & Business Media, 2012.
[79] J. Wang, L. Jiang, Z. Sun, B. Hu, F. Zhang, G. Song, T. Liu, J. Qi, L. Zhang, Research on the surface subsidence monitoring technology based on fiber bragg grating sensing, Photonic Sens. 7 (1) (2017) 20–26.
[80] T. Liu, Y. Wei, G. Song, B. Hu, L. Li, G. Jin, J. Wang, Y. Li, C. Song, Z. Shi, et al., Fibre optic sensors for coal mine hazard detection, Measurement 124 (2018) 211–223.
[81] M. Ghimire, C. Wang, K. Dixon, M. Serrato, In situ monitoring of prestressed concrete using embedded fiber loop ringdown strain sensor, Measurement 124 (2018) 224–232.
[82] G. Rajan, J.S. Vinod, T. Moses, B.G. Prusty, J. Xi, Ballast breakage analysis using FBG acoustic emission measurement system, Geotech. Geol. Eng. 35 (3) (2017) 1239–1247.
[83] D.H. Waters, J. Hoffman, M. Kumosa, Monitoring of overhead transmission conductors subjected to static and impact loads using fiber Bragg grating sensors, IEEE Trans. Instrum. Meas. 68 (2) (2019) 595–605.
[84] S. Zhang, C. Xu, J. Chen, J. Jiang, An experimental evaluation of impact force on a fiber Bragg grating-based device for debris flow warning, Landslides 16 (1) (2019) 65–73.
[85] W. Guo, Y. Chen, F. Xu, Y.Q. Lu, Modeling of the influence of coupling in optical microfiber resonators, Optics Express 20 (13) (2012) 14392–14399.
[86] G. Yan, A.P. Zhang, G. Ma, B. Wang, B. Kim, J. Im, S. He, Y. Chung, Fiber-optic acetylene gas sensor based on microstructured optical fiber Bragg gratings, IEEE Photonics Technol. Lett. 23 (21) (2011) 1588–1590.
[87] W. Zhang, D.J. Webb, Humidity responsivity of poly (methyl methacrylate)-based optical fiber Bragg grating sensors, Optics Lett. 39 (10) (2014) 3026–3029.
[88] F.D. Maria de Fátima, T. de Brito Paixão, E.F.T. Mesquita, N. Alberto, A.R. Frias, R.A. Ferreira, H. Varum, P.F. da Costa Antunes, P.S. de Brito André, Liquid hydrostatic pressure optical sensor based on micro-cavity produced by the catastrophic fuse effect, IEEE Sens. J. 15 (10) (2015) 5654–5658.
[89] L. Chen, W. Zhang, Y. Liu, L. Wang, J. Sieg, B. Wang, Q. Zhou, L. Zhang, T. Yan, Real time and simultaneous measurement of displacement and temperature

using fiber loop with polymer coating and fiber Bragg grating, Rev. Sci. Instrum. 85 (7) (2014) 075002.
[90] M.Q. Chen, Y. Zhao, R.Q. Lv, F. Xia, Hybrid MEFPI/FBG sensor for simultaneous measurement of strain and magnetic field, Optic. Fiber Technol. 39 (2017) 32–36.
[91] G.Y. Chen, G. Brambilla, T.P. Newson, Inspection of electrical wires for insulation faults and current surges using sliding temperature sensor based on optical microfibre coil resonator, Electron. Lett. 49 (1) (2013) 46–47.
[92] A. Dutta, B. Deka, P. Pratim Sahu, Planar waveguide optical sensors.
[93] L. Johnson, F. Leonberger, G. Pratt Jr., Integrated optical temperature sensor, Appl. Phys. Lett. 41 (2) (1982) 134–136.
[94] P. Dumais, C.L. Callender, J.P. Noad, C.J. Ledderhof, Temperature sensors and refractometers using liquid-core waveguide structures monolithically integrated in silica-on-silicon, Photonics North 2008, vol. 7099 (2008) 70991Y, International Society for Optics and Photonics.
[95] R. Kleindienst, S. Sinzinger, Integrated microsystems for optical sensing and imaging applications, Smart Photonic and Optoelectronic Integrated Circuits XVIII, vol. 9751 (2016) 975110, International Society for Optics and Photonics.
[96] C. Gutiérrez-Martínez, J. Santos-Aguilar, J. Meza-Pérez, A. Morales-Díaz, Novel electric field sensing scheme using integrated optics linbo 3 unbalanced mach-zehnder interferometers and optical delay-modulation, J. Lightw. Technol. 35 (1) (2017) 27–33.
[97] C.A. Díaz, C.A. Marques, M.F.F. Domingues, M.R. Ribeiro, A. Frizera-Neto, M.J. Pontes, P.S. André, P.F. Antunes, A cost-effective edge-filter based FBG interrogator using catastrophic fuse effect micro-cavity interferometers, Measurement 124 (2018) 486–493.
[98] Y. Liu, C. Meng, A.P. Zhang, Y. Xiao, H. Yu, L. Tong, Compact microfiber bragg gratings with high-index contrast, Optics Lett. 36 (16) (2011) 3115–3117.
[99] D.-S. Xu, A new measurement approach for small deformations of soil specimens using fiber bragg grating sensors, Sensors 17 (5) (2017) 1016.
[100] F.J. Dutz, V. Stephan, G. Marchi, A.W. Koch, J. Roths, H.P. Huber, Fabrication of locally micro-structured fiber Bragg gratings by fs-laser machining, Appl. Phys. A 124 (6) (2018) 426.
[101] S.M. Melle, K. Liu, et al., Practical fiber-optic Bragg grating strain gauge system, Appl. Optics 32 (19) (1993) 3601–3609.
[102] B. Bell, S. Stankowski, B. Moser, V. Oliva, C. Stieger, L.P. Nolte, M. Caversaccio, S. Weber, Integrating optical fiber force sensors into microforceps for ORL microsurgery, 2010 Annual International Conference of the IEEE Engineering in Medicine and Biology (2010) 1848–1851, IEEE.
[103] A. Iadicicco, M. Della Pietra, M. Alviggi, V. Canale, S. Campopiano, Deflection monitoring method using fiber Bragg gratings applied to tracking particle detectors, IEEE Photonics J. 6 (6) (2014) 1–10.
[104] L. Zhang, Y. Liu, X. Gao, Z. Xia, High temperature strain sensor based on a fiber Bragg grating and rhombus metal structure, Appl. Optics 54 (28) (2015) E109–E112.
[105] R. Min, B. Ortega, C. Broadway, X. Hu, C. Caucheteur, O. Bang, P. Antunes, C. Marques, Microstructured PMMA POF chirped Bragg gratings for strain sensing, Optic. Fiber Technol. 45 (2018) 330–335.
[106] R. Li, Y. Chen, Y. Tan, Z. Zhou, T. Li, J. Mao, Sensitivity enhancement of FBG-based strain sensor, Sensors 18 (5) (2018) 1607.
[107] Y.L. Park, S. Elayaperumal, B. Daniel, S.C. Ryu, M. Shin, J. Savall, R.J. Black, B. Moslehi, M.R. Cutkosky, Real-time estimation of 3-D needle shape and deflection for MRI-guided interventions, IEEE/ASME Trans. Mechatron. 15 (6) (2010) 906–915.
[108] R.M. Liu, D.K. Liang, A. Asundi, Small diameter fiber Bragg gratings and applications, Measurement 46 (9) (2013) 3440–3448.
[109] C. Shi, T. Li, H. Ren, A millinewton resolution fiber Bragg grating-based catheter two-dimensional distal force sensor for cardiac catheterization, IEEE Sens. J. 18 (4) (2017) 1539–1546.
[110] L. Xiong, G. Jiang, Y. Guo, H. Liu, A three-dimensional fiber Bragg grating force sensor for robot, IEEE Sens. J. 18 (9) (2018) 3632–3639.
[111] A. Gao, Y. Zhou, L. Cao, Z. Wang, H. Liu, Fiber Bragg grating-based triaxial force sensor with parallel flexure hinges, IEEE Trans. Ind. Electron. 65 (10) (2018) 8215–8223.
[112] B. Gonenc, J. Chae, P. Gehlbach, R.H. Taylor, I. Iordachita, Towards robot-assisted retinal vein cannulation: a motorized force-sensing microneedle integrated with a handheld micromanipulator, Sensors 17 (10) (2017) 2195.
[113] B. Gonenc, A. Chamani, J. Handa, P. Gehlbach, R.H. Taylor, I. Iordachita, 3-DOF force-sensing motorized micro-forceps for robot-assisted vitreoretinal surgery, IEEE Sens. J. 17 (11) (2017) 3526–3541.
[114] H. Suzuki, H. Masuda, K. Hongo, R. Horie, S. Yajima, Y. Itotani, M. Fujita, K. Nagasaka, Development and testing of force-sensing forceps using FBG for bilateral micro-operation system, IEEE Robot. Autom. Lett. 3 (4) (2018) 4281–4288.
[115] X. Chen, C. Zhang, D.J. Webb, G.D. Peng, K. Kalli, Bragg grating in a polymer optical fibre for strain, bend and temperature sensing, Meas. Sci. Technol. 21 (9) (2010) 094005.
[116] S. Elayaperumal, J.C. Plata, A.B. Holbrook, Y.L. Park, K.B. Pauly, B.L. Daniel, M.R. Cutkosky, Autonomous real-time interventional scan plane control with a 3-D shape-sensing needle, IEEE Trans. Med. Imaging 33 (11) (2014) 2128–2139.
[117] S. Elayaperumal, J.H. Bae, D. Christensen, M.R. Cutkosky, B.L. Daniel, R.J. Black, J.M. Costa, F. Faridian, B. Moslehi, MR-compatible biopsy needle with enhanced tip force sensing, 2013 World Haptics Conference (WHC) (2013) 109–114, IEEE.
[118] M. Royon, D. Piétroy, E. Marin, A. Saulot, A thermomechanical sensor using photo-inscribed volume Bragg gratings, Tribol. Int. 115 (2017) 417–423.
[119] U. Nawrot, T. Geernaert, B. De Pauw, D. Anastasopoulos, E. Reynders, G. De Roeck, F. Berghmans, Development of a mechanical strain amplifying transducer with Bragg grating sensor for low-amplitude strain sensing, Smart Mater. Struct. 26 (7) (2017) 075006.
[120] R. Li, Y. Chen, Y. Tan, Z. Zhou, T. Li, J. Mao, Sensitivity enhancement of FBG-based strain sensor, Sensors 18 (5) (2018) 1607.
[121] Y.J. Rao, Z.L. Ran, Optic fiber sensors fabricated by laser-micromachining, Optic. Fiber Technol. 19 (6) (2013) 808–821.
[122] G. Marchi, V. Stephan, F.J. Dutz, B. Hopf, L. Polz, H.P. Huber, J. Roths, Femtosecond laser machined micro-structured fiber Bragg grating for simultaneous temperature and force measurements, J. Lightw. Technol. 34 (19) (2016) 4557–4563.
[123] W. He, L. Zhu, W. Zhang, F. Liu, M. Dong, Point-by-point femtosecond-laser inscription of 2-μm-wavelength-band FBG through fiber coating, IEEE Photonics J. 11 (1) (2019) 1–8.
[124] C.R. Liao, D.N. Wang, Y. Wang, Microfiber in-line Mach-Zehnder interferometer for strain sensing, Optics Lett. 38 (5) (2013) 757–759.
[125] C. Thondagere, A. Kaushalram, T. Srinivas, G. Hegde, Mathematical modeling of optical MEMS differential pressure sensor using waveguide Bragg gratings embedded in Mach Zehnder interferometer, J. Optics 20 (8) (2018) 085802.
[126] C. Yin, Z. Cao, Z. Zhang, T. Shui, R. Wang, J. Wang, L. Lu, S. Zhen, B. Yu, Temperature-independent ultrasensitive Fabry-Pérot all-fiber strain sensor based on a bubble-expanded microcavity, IEEE Photonics J. 6 (4) (2014) 1–9.
[127] F.C. Favero, L. Araujo, G. Bouwmans, V. Finazzi, J. Villatoro, V. Pruneri, Spheroidal Fabry-Perot microcavities in optical fibers for high-sensitivity sensing, Optics Express 20 (7) (2012) 7112–7118.
[128] Q. Liu, Z.L. Ran, Y.J. Rao, S.C. Luo, H.Q. Yang, Y. Huang, Highly integrated FP/FBG sensor for simultaneous measurement of high temperature and strain, IEEE Photonics Technol. Lett. 26 (17) (2014) 1715–1717.
[129] S. Liu, Y. Wang, C. Liao, G. Wang, Z. Li, Q. Wang, J. Zhou, K. Yang, X. Zhong, J. Zhao, et al., High-sensitivity strain sensor based on in-fiber improved Fabry-Perot interferometer, Optics Lett. 39 (7) (2014) 2121–2124.
[130] S. Liu, K. Yang, Y. Wang, J. Qu, C. Liao, J. He, Z. Li, G. Yin, B. Sun, J. Zhou, et al., High-sensitivity strain sensor based on in-fiber rectangular air bubble, Sci. Rep. 5 (2015) 7624.
[131] J.Y. Li, X.G. Huang, G.M. Cheng, L.-X. Chen, X.-M. Jin, Integration of a micro Fabry-Perot cavity and a fiber Bragg grating sensor for simultaneous measurement of stress and temperature, Microw. Optic. Technol. Lett. 55 (10) (2013) 2440–2444.
[132] Z. Bai, S. Gao, M. Deng, Z. Zhang, M. Li, F. Zhang, C. Liao, Y. Wang, Y. Wang, Bidirectional bend sensor employing a microfiber-assisted U-shaped Fabry-Perot cavity, IEEE Photonics J. 9 (3) (2017) 1–8.
[133] X. Zhang, W. Peng, L.Y. Shao, W. Pan, L. Yan, Strain and temperature discrimination by using temperature-independent FPI and FBG, Sens. Actuators A: Phys. 272 (2018) 134–138.
[134] H. Zhao, K. O'Brien, S. Li, R.F. Shepherd, Optoelectronically innervated soft prosthetic hand via stretchable optical waveguides, Sci. Robot. 1 (1) (2016) eaai7529.
[135] G.Y. Chen, S. Shahnia, T.M. Monro, D.G. Lancaster, Force sensors using the skew-ray-probed plastic optical fibers, IEEE Photonics J. 10 (3) (2018) 1–8.
[136] P. Puangmali, H. Liu, L.D. Seneviratne, P. Dasgupta, K. Althoefer, Miniature 3-axis distal force sensor for minimally invasive surgical palpation, IEEE/ASME Trans. Mechatron. 17 (4) (2012) 646–656.
[137] O. Al-Mai, M. Ahmadi, J. Albert, A compliant 3-axis fiber-optic force sensor for biomechanical measurement, IEEE Sens. J. 17 (20) (2017) 6549–6557.
[138] M. Ghimire, C. Wang, Highly sensitive fiber loop ringdown strain sensor with low temperature sensitivity, Meas. Sci. Technol. 28 (10) (2017) 105101.
[139] L. Tong, Micro/nanofibre optical sensors: challenges and prospects, Sensors 18 (3) (2018) 903.
[140] L. Tong, R.R. Gattass, J.B. Ashcom, S. He, J. Lou, M. Shen, I. Maxwell, E. Mazur, Subwavelength-diameter silica wires for low-loss optical wave guiding, Nature 426 (6968) (2003) 816.
[141] L. Tong, F. Zi, X. Guo, J. Lou, Optical microfibers and nanofibers: a tutorial, Optics Commun. 285 (23) (2012) 4641–4647.
[142] B.O. Guan, J. Li, L. Jin, Y. Ran, Fiber bragg gratings in optical microfibers, Optic. Fiber Technol. 19 (6) (2013) 793–801.
[143] T. Wieduwilt, S. Brückner, H. Bartelt, High force measurement sensitivity with fiber Bragg gratings fabricated in uniform-waist fiber tapers, Meas. Sci. Technol. 22 (7) (2011) 075201.
[144] W. Luo, J.L. Kou, Y. Chen, F. Xu, Y.Q. Lu, Ultra-highly sensitive surface-corrugated microfiber Bragg grating force sensor, Appl. Phys. Lett. 101 (13) (2012) 133502.
[145] J.-L. Kou, S.-J. Qiu, F. Xu, Y.-Q. Lu, Y. Yuan, G. Zhao, Miniaturized metal-dielectric-hybrid fiber tip grating for refractive index sensing, IEEE Photonics Technol. Lett. 23 (22) (2011) 1712–1714.
[146] K.M. Chung, Z. Liu, C. Lu, H.Y. Tam, Highly sensitive compact force sensor based on microfiber Bragg grating, IEEE Photonics Technol. Lett. 24 (8) (2012) 700–702.
[147] Y. Ran, S. Gao, L. Jin, L.P. Sun, Y.Y. Huang, J. Li, B. Guan, Sensitive strain sensor based on regenerated microfiber Bragg grating for high temperature environment, Fifth Asia-Pacific Optical Sensors Conference, vol. 9655 (2015) 96552V, International Society for Optics and Photonics.

[148] J. Lou, Y. Wang, L. Tong, Microfiber optical sensors: a review, Sensors 14 (4) (2014) 5823–5844.
[149] Q. Wang, J.Y. Jing, B.T. Wang, S. Li, Recent progress and applications of optical microfiber and nanofiber devices, Instrum. Sci. Technol. 47 (2) (2019) 117–139.
[150] B. Bhola, H.C. Song, H. Tazawa, W.H. Steier, Polymer microresonator strain sensors, IEEE Photonics Technol. Lett. 17 (4) (2005) 867–869.
[151] Y. Chen, S.C. Yan, X. Zheng, F. Xu, Y.Q. Lu, A miniature reflective micro-force sensor based on a microfiber coupler, Optics Express 22 (3) (2014) 2443–2450.
[152] P. Youplao, M. Tasakorn, T. Phattaraworamet, The simulation of a force in micro-scale sensing employing an optical double ring resonator system, Pertanika J. Sci. Technol. 26 (1) (2018).
[153] W. Li, Z. Hu, X. Li, W. Fang, X. Guo, L. Tong, J. Lou, High-sensitivity microfiber strain and force sensors, Optics Commun. 314 (2014) 28–30.
[154] G. Statkiewicz-Barabach, D. Kowal, M.K. Szczurowski, P. Mergo, W. Urbanczyk, Hydrostatic pressure and strain sensitivity of long period grating fabricated in polymer microstructured fiber, IEEE Photonics Technol. Lett. 25 (5) (2013) 496–499.
[155] A. Iadicicco, S. Campopiano, A. Cutolo, Characterization of long period gratings in hollow core fiber fabricated via electrode arc discharge, 2014 Fotonica AEIT Italian Conference on Photonics Technologies (2014) 1–3, IEEE.
[156] A. Iadicicco, R. Ranjan, S. Campopiano, Fabrication and characterization of long-period gratings in hollow core fibers by electric arc discharge, IEEE Sens. J. 15 (5) (2015) 3014–3020.
[157] A. Candiani, M. Konstantaki, A. Pamvouxoglou, S. Pissadakis, A shear sensing pad, based on ferrofluidic actuation in a microstructured optical fiber, IEEE J. Sel. Topics Quantum Electron. 23 (2) (2017) 210–216.
[158] H. Gong, C.C. Chan, L. Chen, X. Dong, Strain sensor realized by using low-birefringence photonic-crystal-fiber-based Sagnac loop, IEEE Photonics Technol. Lett. 22 (16) (2010) 1238–1240.
[159] W. Qian, C.L. Zhao, X. Dong, W. Jin, Intensity measurement based temperature-independent strain sensor using a highly birefringent photonic crystal fiber loop mirror, Optics Commun. 283 (24) (2010) 5250–5254.
[160] D.W. Duan, Y.J. Rao, Y.S. Hou, T. Zhu, Microbubble based fiber-optic Fabry-Perot interferometer formed by fusion splicing single-mode fibers for strain measurement, Appl. Optics 51 (8) (2012) 1033–1036.
[161] L.M. Hu, C.C. Chan, X.Y. Dong, Y.P. Wang, P. Zu, W.C. Wong, W.W. Qian, T. Li, Photonic crystal fiber strain sensor based on modified Mach-Zehnder interferometer, IEEE Photonics J. 4 (1) (2012) 114–118.
[162] C. Yang, H. Zhang, H. Liang, Y. Miao, B. Liu, Z. Wang, Y. Liu, Selectively liquid-infiltrated microstructured optical fiber for simultaneous temperature and force measurement, IEEE Photonics J. 6 (2) (2014) 1–8.
[163] Y. Zhou, B.J. Nelson, Adhesion force modeling and measurement for micromanipulation Microrobotics and Micromanipulation, vol. 3519, International Society for Optics and Photonics, 1998, pp. 169–181.
[164] X.J. Zhang, S. Zappe, R.W. Bernstein, O. Sahin, C.C. Chen, M. Fish, M.P. Scott, O. Solgaard, Micromachined silicon force sensor based on diffractive optical encoders for characterization of microinjection, Sens. Actuators A: Phys. 114 (2) (2004) 197–203.
[165] X. Zhang, Silicon microsurgery-force sensor based on diffractive optical MEMS encoders, Sens. Rev. 24 (1) (2004) 37–41.
[166] R. Araki, T. Abe, H. Noma, M. Sohgawa, Electromotive manipulator control by detection of proximity, contact, and slipping using MEMS multiaxial tactile sensor, Electr. Eng. Jpn. 204 (2) (2018) 44–49.
[167] M. Power, A.J. Thompson, S. Anastasova, G.Z. Yang, A monolithic force-sensitive 3D microgripper fabricated on the tip of an optical fiber using 2-photon polymerization, Small 14 (16) (2018) 1703964.
[168] A.J. Thompson, M. Power, G.Z. Yang, Micro-scale fiber-optic force sensor fabricated using direct laser writing and calibrated using machine learning, Optics Express 26 (11) (2018) 14186–14200.
[169] H. Li, X. Zhang, B. Zhu, Y. Lu, H. Wu, Micro-motion detection of the 3-DOF precision positioning stage based on iterative optimized template matching, Appl. Optics 56 (34) (2017) 9435–9443.
[170] H. Li, B. Zhu, Z. Chen, X. Zhang, Realtime in-plane displacements tracking of the precision positioning stage based on computer micro-vision, Mech. Syst. Signal Process. 124 (2019) 111–123.
[171] H. Wu, X. Zhang, R. Wang, Z. He, Displacement measurement of the compliant positioning stage based on a computer micro-vision method, AIP Adv. 6 (2) (2016) 025009.
[172] X. Zhang, X. Zhang, H. Wu, J. Gan, H. Li, A high accuracy algorithm of displacement measurement for a micro-positioning stage, AIP Adv. 7 (5) (2017) 055301.
[173] X. Zhang, X. Zhang, H. Wu, H. Li, J. Gan, A robust rotation-invariance displacement measurement method for a micro-/nano-positioning system, Meas. Sci. Technol. 29 (5) (2018) 055402.
[174] W. Brenner, M. Ferros, D. Andrijasevic, H. Hotzendorfer, I. Giouroudi, Design of a microgripping system with visual and force feedback for MEMS applications, The Institution of Engineering and Technology Seminar on MEMS Sensors and Actuators 2006 (2006) 243–250, IET.
[175] A.N. Reddy, N. Maheshwari, D.K. Sahu, G. Ananthasuresh, Miniature compliant grippers with vision-based force sensing, IEEE Trans. Robot. 26 (5) (2010) 867–877.
[176] H. Xie, S. Régnier, High-efficiency automated nanomanipulation with parallel imaging/manipulation force microscopy, IEEE Trans. Nanotechnol. 11 (1) (2012) 21–33.
[177] N. Yu, M. Nakajima, Q. Shi, Z. Yang, H. Wang, L. Sun, Q. Huang, T. Fukuda, Characterization of the resistance and force of a carbon nanotube/metal side contact by nanomanipulation, Scanning 2017 (1) (2017) 5910734.
[178] F. Karimirad, B. Shirinzadeh, W. Yan, S. Fatikow, A vision-based methodology to dynamically track and describe cell deformation during cell micromanipulation, Int. J. Optomechatron. 7 (1) (2013) 33–45.
[179] F. Karimirad, S. Chauhan, B. Shirinzadeh, Vision-based force measurement using neural networks for biological cell microinjection, J. Biomech. 47 (5) (2014) 1157–1163.
[180] K.O. Hill, G. Meltz, Fiber Bragg grating technology fundamentals and overview, J. Lightw. Technol. 15 (8) (1997) 1263–1276.

Biographies

Haoyan Zang was born in 1996. She received a bachelor's degree from the South China University of Technology. She is currently pursuing her Ph.D. degree at the School of Mechanical and Automotive Engineering, South China University of Technology, Guangzhou, China. Her research interest is in the field of the design and application of force sensors for the micro/nano manipulation systems.

Xianmin Zhang was born in 1964. He received the Ph.D. degree from the Beijing University of Aeronautics and Astronautics, Beijing, China, in 1993. He was the Dean of the College of Mechanical and Automotive Engineering, South China University of Technology, Guangzhou, China, in 2013. He has been a Professor with the South China University of Technology since 2003. His current research interests include mechanism design and dynamics, and inspection technique.

Benliang Zhu received the Ph.D. degree in mechanical engineering from the South China University of Technology, Guangzhou, China, in 2014. He is currently an Associate Professor with the South China University of Technology. His current research interests involve MEMS technique, precision positioning, and manipulation in the microscale and nanoscale.

Sergej Fatikow studied electrical engineering and computer science at the Ufa Aviation Technical University in Russia, where he received his doctoral degree in 1988. Since 2001 he is a full professor in the Department of Computing Science and Head of the Division for Microrobotics and Control Engineering (AMiR) at the University of Oldenburg, Germany. His research interests include micro- and nanorobotics automation at nanoscale, nanohandling inside SEM, AFM-based nanohandling, sensor feedback at nanoscale, and neurofuzzy robot control.